LIGHT SCATTERING IN BINARY GAS MIXTURES: EVIDENCE OF FAST AND SLOW SOUND MODES

LUO HONGDA, B. Sc.

LIGHT SCATTERING IN BINARY GAS MIXTURES: EVIDENCE OF FAST AND SLOW SOUND MODES

By

Luo Hongda, B.Sc

A thesis submitted in partial fulfillment
of the requirements for the degree of
Master of Science

Department of Physics
Memorial University of Newfoundland

August 1990

St. John's Newfoundland

ISBN 0-315-65329-9

ABSTRACT

In this thesis Brillouin scattering data are presented for three different binary gas mixtures composed of species with widely different masses, i.e. Ar + H_2 ($m_{Ar}/m_{H_2} \simeq 20$), SF_6 + CH_4 ($m_{SF_6}/m_{CH_4} \simeq 9$), and SF_6 + H_2 ($m_{SF_6}/m_{H_2} \simeq 73$). Under the experimental conditions predicted by the theory a fast sound mode contribution to the light scattering spectra of Ar + H_2 mixtures has been detected. Unlike the ordinary sound mode the fast sound mode propagates only in the light component with a velocity higher than that obtained using hydrodynamic theory. However, the attempts to observe the same effect in mixtures of SF_6 + CH_4 under similar conditions were unsuccessful. An analogous slow sound mode contribution to the spectra of SF_6 + H_2 mixtures has been clearly identified and it was found this mode was, in general, much easier to detect.

A new parameter called the effective mean free path was also introduced in order to obtain a more consistent characterization of the dynamical behavior in binary mixtures with disparate masses.

ACKNOWLEDGEMENTS

I would like to express my sincere gratitudes to my supervisor Dr. M. J. Clouter for guidance at every step of this experiment. His experience has been of great help to me throughout this project and in the preparation of this thesis.

I wish to thank my supervisor Dr. H. Kiefte for his careful reading of this thesis, his encouragement and valuable help in the final stage of the thesis.

In particular, I am grateful to Dr. A. Campa of the Rockefeller University, and Dr. J. A. Zollweg of the School of Chemical Engineering, Cornell University for sending me the theoretical calculations concerning our experiment.

Thanks go to Dr. J.K.C. Lewis and Dr. N. Rich for their helpful discussion and advice and to my friends V. Askarpour and Dr. Richard R. J. Goulding for what they have done for me during my stay at Memorial University of Newfoundland.

I also wish to gratefully acknowledge the financial support of my work from Memorial University of Newfoundland.

CONTENTS

LIST OF FIGURES

Chapter 1. Introduction

§. 1.1. FLUCTUATIONS & BRILLOUIN SCATTERING

The scattering of light generally arises as the result of opt'cal inhomogeneities in the scattering medium. The physical reasons for the generation of optical inhomogeneities in the scattering medium are various. For example, contamination by foreign substances is one possibility. However, even in substances which are completely free from any kind of foreign contaminants, scattered light can be observed as the result of the statistical character of thermal motion. In this case, the optical inhomogeneities are caused by the local fluctuations of the optical dielectric constant, which are directly brought about, in turn, by the fluctuations in local density of the substance. In contrast with the impurity scattering and Raman scattering, this kind of light scattering, arising from random thermal fluctuations is called Brillouin scattering[1].

According to Brillouin, the spontaneous density fluctuations in the medium can be decomposed into different plane-wave Fourier

components. These plane-waves propagating in the medium cause a periodic density change along the propagation directions. Scattered light is brought about by the diffraction of the incident plane monochromatic light wave which is considered to be diffracted by the density maxima of the thermal sound wave in the same way as X-rays are scattered by a crystal. If $\mathbf{k}_0$ is the wave vector of the incident light, $\mathbf{k}_s$ is the wave vector of the scattered light and K is the wave vector of the Kth Fourier component of the sound wave caused by the spontaneous local density fluctuations of the medium in direction $\hat{K}$, then the condition for scattering is given by the Bragg relation [Fig.1.1]

$$K = \pm (k_0 - k_s), \tag{1.1}$$

where the choice of signs refers to either of two oppositely directed sound waves. Because the density maxima are travelling with the velocity of sound in the fluid (fluid refers to both gas and liquid here), the frequency of the scattered light will consequently be Doppler shifted. If ω_0 is the angular frequency of the incident light wave, ω_s is that of the scattered wave, v_s is the sound velocity, θ is the scattering angle, n is the refractive index of the medium, and c is the velocity of light in vacuum, then to a high degree of approximation, the frequency shift is given by the well-known Brillouin relation

$$\Delta\omega = \omega_s - \omega_0 = \pm \frac{2\omega_0 v_s n}{c} \sin(\frac{\theta}{2}). \tag{1.2}$$

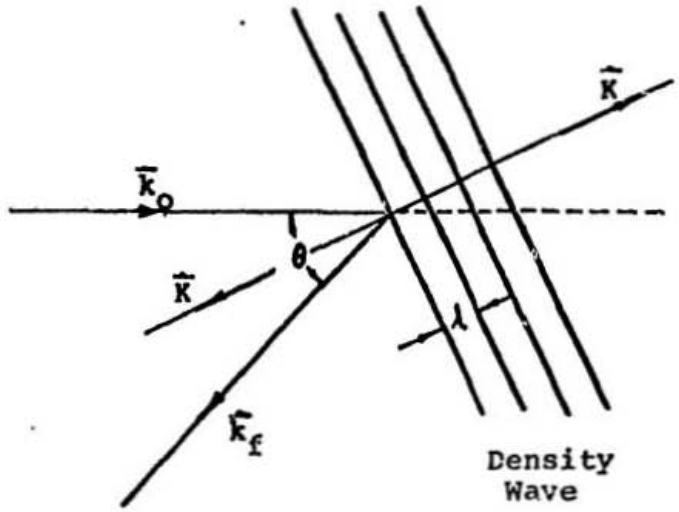

Fig. 1.1 Classical picture of Bragg reflection. The incident light wave is scattered by the density wave in the medium. k_o is the wave vector of the incident light, k_f is the wave vector of the scattered light, K is the wave vector of the density wave, and θ is the scattering angle.

Although sound waves of many different wavelengths and any propagation direction are present in the medium, in an actual light scattering experiment for each scattering angle θ other than zero only the sound waves with wave vector given by (1.1) can be observed. According to (1.2), the scattering spectrum consists of only two sharp lines with frequency shifts of $\pm\Delta\omega$, respectively, from the central frequency ω_0. In reality, the spectrum of the scattered light also includes a central line with no frequency shift. Landau and Placzek[2] gave the following explanation for the origin of the central peak. They pointed out that the thermal fluctuations in a fluid were composed of two parts, namely, isobaric fluctuations caused by entropy fluctuations at constant pressure, and adiabatic fluctuations caused by pressure fluctuations at constant entropy. Fluctuations of the first type are unorganized in time, so they are not propagated in the form of waves and consequently the central line can be explained as elastic Rayleigh scattering. On the other hand, the pressure fluctuations represent random local compressions or rarefactions which, as a consequence of the elastic properties of the medium, do not remain fixed but travel through the fluid and give rise to a shifted doublet. Because of the existence of dissipative processes which damp out the elastic waves in the medium, the doublet components have nonzero line widths. The nonzero width of the central line can be explained in terms of heat conduction and diffusion. A typical Brillouin spectrum is shown in Fig. 1.2.

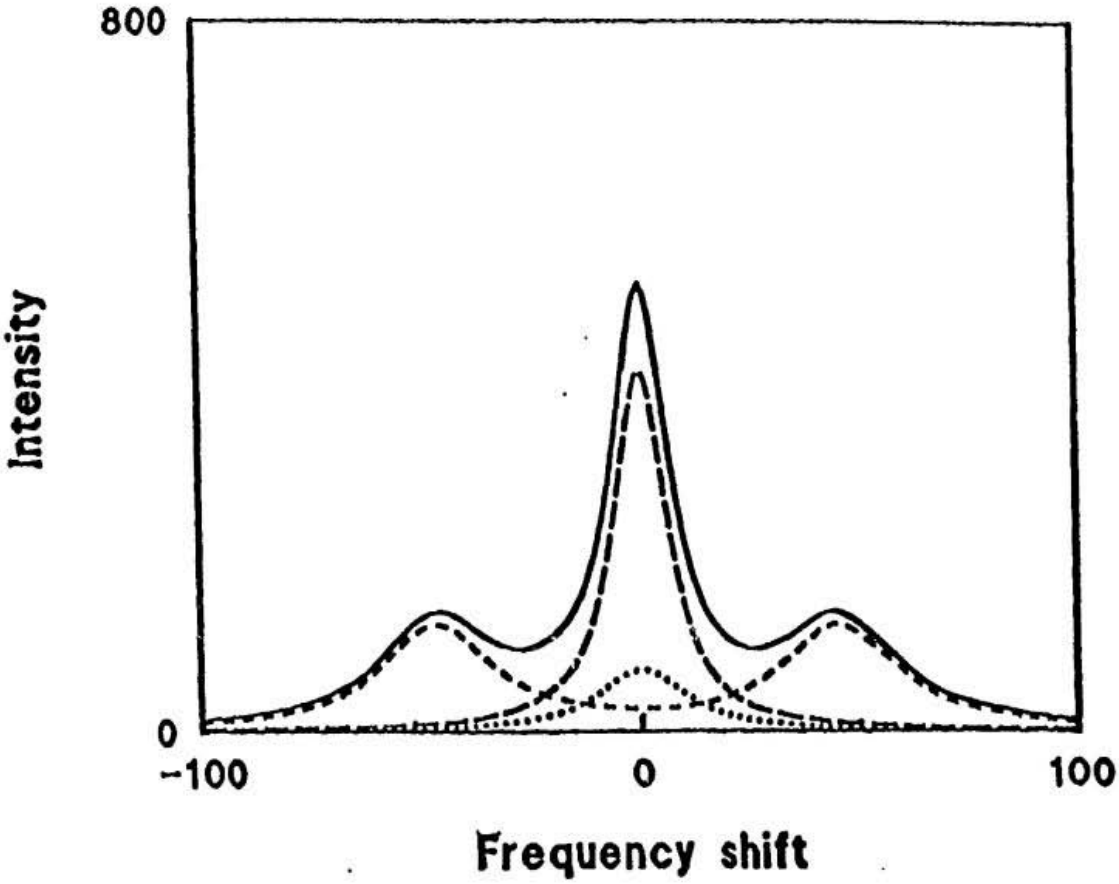

Fig. 1.2 Schematic representation of the scattered light spectrum from a fluid: long-dashed line represents the undisplaced Rayleigh component; short-dashed line represents the Stokes and anti-Stokes Brillouin components; dotted line indicates the non-propagating fourth component which is much less intense than others[1]; solid line indicates the aggregate intensity distribution in the scattered spectrum.

§. 1.2. THE MEAN FREE PATHS IN BINARY MIXTURES

Theoretically the spontaneous density fluctuations in the medium can be decomposed into density plane-waves of different wave lengths. In reality, however, only those density waves with wave lengths larger than or comparable to the mean free path ℓ exist in the medium. Usually the product of K and mean free path ℓ is used to characterize the conditions of the samples(see §. 1.3). The mean free path in a low-density one-component fluid is given by

$$\ell = (\sqrt{2}\pi n\sigma^2)^{-1}, \tag{1.3}$$

where σ is the hard sphere diameter of the particle and n is the number density.

For the binary mixtures the situation is somewhat complicated because there are several possible definitions for the mean free path. For example, it is possible to define a mean free path with respect to collisions between the specific types of particles. Here we introduce two mean free paths ℓ_1 and ℓ_2 defined by[3]

$$\ell_1 = (\ell_{11}^{-1} + \ell_{12}^{-1})^{-1}, \tag{1.4a}$$

$$\ell_2 = (\ell_{21}^{-1} + \ell_{22}^{-1})^{-1}, \tag{1.4b}$$

where ℓ_{ij} (i,j = 1,2), the average distance travelled by a

particle of species i between its two successive collisions with particles of species j, is given by the following relation

$$\ell_{ij} = [\pi n_j \sigma_{ij}^2 (1 + m_i/m_j)^{1/2}]^{-1}, \quad (i,j = 1,2) \qquad (1.5)$$

where n_i, σ_i and m_i represent the number density, hard sphere diameter and mass of species i, $\sigma_{ij} = (\sigma_i + \sigma_j)/2$.

If a particle of species 1 travels a distance L, according to the definition of ℓ_{ij}, the average numbers of collisions it experiences with particles of species 1 and 2 are given by L/ℓ_{11} and L/ℓ_{12} respectively. The average total numbers of collisions is given by $L/\ell_{11} + L/\ell_{12}$. Hence ℓ_1, which equals to $L/[L/\ell_{11} + L/\ell_{12}]$, can be understood as the average distance between two successive collisions experienced by particles of species 1. However, as we will see in Chapter 4, for the binary mixtures with large mass difference ℓ_1 and ℓ_2 are insufficient to characterize the conditions of binary fluids. A possible solution is via the "effective mean free path" which will be defined and discussed later.

§. 1.3. HYDRODYNAMIC & KINETIC REGIMES

In a simple fluid, a dimensionless parameter $K\ell$ (ℓ is the mean free path of particles in the fluid) is used to characterize

the nature of the density fluctuations to be probed[4]. The individual particles in the fluid travel a finite distance ℓ between inter-particle collisions which cause local density fluctuations. Since K is the wave vector of the fluctuations to be probed, a small value for $K\ell$ means that within the length scale 1/K (the wave-length of thermal sound wave) many collisions occur. So in the limit of $K\ell \ll 1$ (hydrodynamic regime), the deviation from local thermodynamic equilibrium is very small and hydrodynamic theory can be used. On the other hand, for $K\ell \sim 1$ (kinetic regime), particles undergo few collisions over the 1/K length scale and the local equilibrium assumption ceases to be valid. One must use kinetic theory to obtain a more general and more microscopic description. The region $K\ell \gg 1$ is the free-streaming region and yields the well-known Doppler profile, which is not of interest here.

In a binary fluid, the situation is more complicated since there are several possible definitions of the mean free path. More detailed discussions will be given in Chapter 4.

§. 1.4. DYNAMICS OF DISPARATE-MASS GAS MIXTURES

The Fast and Slow Sound Modes

The investigation of binary disparate-mass mixtures, where the two components have very different masses, began in 1960. At

that time Grad[5] pointed out that in a dilute disparate-mass mixture the slow exchange of kinetic energy between two components should lead to two temperatures: one is associated with the light component and another is associated with the heavy component. In the late 1970s, when Huck and Johnson[6] studied the behavior of forced sound modes in dilute binary disparate-mass gas mixtures of xenon and helium ($m_{Xe}/m_{He}\approx 33$), the idea was further developed. In their studies, they predicted the existence of two different forced sound modes, namely a fast sound mode and a slow sound mode. The fast sound mode is associated only with the light component and propagates with a velocity greater than that expected for hydrodynamic behavior of the mixture, while the slow sound mode is just the opposite; it is associated with the heavy component and propagates with a lower velocity. In the experiments conducted by Bowler and Johnson[7] in dilute binary mixtures of He and Xe, a sharp increase in sound velocity was found under an external disturbance with frequencies $\omega > 10^6$ Hz and He mole fractions higher than 0.45. More recently, in 1986, Bosse, Jacucci and Ronchentti[8] found a fast propagating sound mode in computer simulations of LiPb liquid alloys with large atomic mass difference ($m_{Pb}/m_{Li}\approx 30$). They predicted, for high frequencies and large wave numbers beyond the hydrodynamic regime, and under the condition of high concentration of the light component, that the fast sound could be observed by the using inelastic neutron scattering technique. This was confirmed in experiments by Montifrooij, Westerhuij and Haan[9]. In their latest paper, Campa

and Cohen[10] considered light scattering in dilute disparate-mass binary gas mixtures with high concentrations of the light component and predicted that a fast sound mode should also be observed as the presence of side peaks or extended shoulders which are only associated with the lighter component in the scattering cross section for visible light. For a binary mixture, the scattered light intensity can be expressed as a weighted average of partial dynamic structure factors, (see detailed discussion in Chap. 2)

$$I(K,\omega) \propto \alpha_1^2 x_1 S_{11}(K,\omega) + 2\alpha_1\alpha_2\sqrt{x_1 x_2}\, S_{12}(K,\omega) + \alpha_2^2 x_2 S_{22}(K,\omega), \quad (1.6)$$

where subscripts 1 and 2 refer to the lighter and the heavier species respectively, α_i and x_i denote the molecular polarizability and the mole fraction of component i, K and ω are wave number and angular frequency to be probed, $S_{ij}(K,\omega)$ are partial dynamic structure factors. The first and the third terms in (1.6) are associated with the lighter and heavier species alone and the second is a mixed term. As we can see from expression (1.6), the polarizibilities of two components play important roles in light scattering. In order to observe the fast mode which is only associated with the lighter component, α_1/α_2 should be as large as possible (at least comparable). Considering both mass and polarizability ratios, the mixture combination which Campa and Cohen suggested to study was argon and hydrogen with a mass ratio of $m_{Ar}/m_{H_2} \approx 20$ and polarizability ratio of $\alpha_{H_2}/\alpha_{Ar} \approx 0.5$.

Although several light-scattering experiments had previously been conducted on binary disparate-mass gas mixtures by Gornall [11], Clark[12,13] and Letamendia[14], the experimental conditions and the mixtures they chose were unfavorable for the observation of the fast sound mode. For example, in Clark and Letamendia's experiments, they used xenon and helium ($m_{X_e}/m_{H_e}\approx 33$) mixtures with a polarization ratio of $\alpha_{X_e}/\alpha_{H_e}\approx 19.6$, much higher than that of Ar and H_2. Besides this, according to Campa's calculations, in order to observe the fast sound mode the gas density should be much lower and a larger scattering angle is also preferred. In this thesis, we will present recent light scattering results for dilute H_2 and Ar mixtures, which provide evidence for the existence of a fast mode. Our attempts to observe the same effect in mixtures of CH_4 and SF_6 ($m_{SF_6}/m_{CH_4}\approx 9$, $\alpha_{SF_6}/\alpha_{CH_4}\approx 1.8$) were unsuccessful. However, for the gas mixtures SF_6 and H_2 ($m_{SF_6}/m_{H_2}\approx 73$), an analogous slow mode was observed. Compared with the fast mode, it seems that the slow mode is much easier to detect.

Before presenting the experimental results, it is necessary to give a more detailed description of the theory involved in Brillouin scattering. In the following chapter, we will outline the theoretical background pertaining to the thermal light scattering. The experimental aspects will be contained in Chapter 3 (Apparatus & Experimental Procedure) and Chapter 4 (Experimental Results & Discussion).

Chapter 2. Theory

§. 2.1. DENSITY CORRELATION FUNCTIONS & BRILLOUIN SCATTERING

The density fluctuation of fluids is usually described in the language of space-time correlation functions[15]. A space-time correlation function is defined as the thermodynamic average of the product of two dynamical variables, each of which expresses the instantaneous deviation of a fluid property from its equilibrium value at a particular point in space and time. Generally the space-time correlation function is written as

$$C_{AB}(r,t;r',t') = C_0\langle\delta A(r',t')\cdot\delta B(r,t)\rangle = C_{AB}(|r - r'|, t - t'), \qquad (2.1)$$

where

$$\delta A(r,t) = A(r,t) - \langle A(r,t)\rangle,$$
$$\delta B(r,t) = B(r,t) - \langle B(r,t)\rangle,$$

are the fluctuations in the dynamical variables A(r,t) and B(r,t).

The factor C_0 is a constant defined for the convenience of the specific correlation functions. The angle brackets represent averages over the phase coordinates of all the molecules in the fluid with an equilibrium ensemble as the weighting function, i.e.

$$\langle A(r,t)\rangle_N = \frac{1}{Z(\beta,V,N)} \cdot \int d\Gamma\, A(r,t)\cdot e^{-\beta H(\Gamma)}, \qquad (2.2)$$

where Γ collectively indicates all the phase space variables, $H(\Gamma)$ is the Hamiltonian of the system with N particles in volume V, $\beta=(k_B T)^{-1}$, and $Z(\beta,N,V)$ is the partition function of the system. A space-time correlation function is therefore a function of space and time, and it describes the thermal fluctuations which exist spontaneously in the equilibrium system.

Using classical electrodynamic theory the relation between the appropriate correlation functions and the intensity of Brillouin scattering can be obtained. In order to simplify the discussion we assume that the fluids are composed of optically isotropic molecules, e.g. the inert gases. In this case the fluctuations of the dielectric constant caused by orientations of the molecules in the medium do not need to be considered.

Considering a fluid with an average dielectric constant ϵ_0, the dielectric constant will fluctuate from place to place and from time to time giving rise to inhomogeneities. The instantaneous dielectric constant $\epsilon(r,t)$ can be assumed to be

equal to the average ϵ_0 plus a fluctuation part $\Delta\epsilon(\mathbf{r},t)$, i.e.

$$\epsilon(\mathbf{r},t) = \epsilon_0 + \Delta\epsilon(\mathbf{r},t), \tag{2.3}$$

where $\mathbf{r}$ is the position in the scattering medium. The volume of the medium is assumed to be large so that surface effects may be neglected. Because the molecules are isotropic, ϵ and $\Delta\epsilon$ are simplified to be scalars instead of tensors[16].

Using this local dielectric constant in the Maxwell equations for a nonconducting, nonmagnetic medium, we have

$$\begin{cases} \nabla \times \nabla \times \mathbf{E} = -(1/c^2)(\partial^2 \mathbf{D}/\partial t^2) \\ \nabla \cdot \mathbf{D} = 0 \end{cases} \tag{2.4}$$

where $\mathbf{E}$ is the electric field vector in the medium, and $\mathbf{D}$ is the Maxwell displacement vector which satisfies the following relation

$$\mathbf{D} = \epsilon(\mathbf{r},t) \cdot \mathbf{E}. \tag{2.5}$$

The equations that need to be solved are, therefore

$$\begin{cases} \nabla^2 \mathbf{E} - \nabla(\nabla \cdot \mathbf{E}) - (1/c^2) \cdot [\partial^2(\epsilon \mathbf{E})/\partial t^2] = 0 \\ \nabla \cdot (\epsilon \mathbf{E}) = 0. \end{cases} \tag{2.6}$$

In classical electrodynamic perturbation theory, the scattered electric field $\mathbf{E}$ can be expanded in terms of the incident field $\mathbf{E}_0$ plus higher order terms which only include the light scattered in

other than the direction of the incident light, i.e.

$$E = E_0 + E_1 + E_2 + \cdots\cdots\cdots. \qquad (2.7)$$

Here we assume that the intensity of scattered light with scattering angle $\theta \neq 0$ is small compared to the intensity of the incident light; this condition can be generally realized in gases at not very high pressures.

Substituting equations (2.3) and (2.7) into equations (2.6) and setting sums of the same order of magnitude equal to zero, we obtain a series of equations:

$$\nabla^2 E_0 - \frac{\varepsilon_0}{c^2} \cdot \frac{\partial^2 E_0}{\partial t^2} = 0 \qquad (2.8a)$$

$$\nabla^2 E_1 - \frac{\varepsilon_0}{c^2} \cdot \frac{\partial^2 E_1}{\partial t^2} = \frac{1}{c^2} \cdot \frac{\partial^2 [(\Delta\varepsilon) E_0]}{\partial t^2} - \frac{\nabla[\nabla\cdot(\Delta\varepsilon)E_0]}{\varepsilon_0} \qquad (2.8b)$$

.....etc.,

E_0, which represents the incident light wave will (according to the approximation) be transmitted through the fluid without attenuation. E_1 can be considered as the result of a single scattering process: i.e. in the quantum mechanical description, photons represented by E_1 are scattered only once by phonons[17]. The term of most interest in (2.7) is E_1, the single scattering term. The contributions of E_2 and other higher order scattering

terms are very small except in the neighbourhood of a critical point.

The incident field is assumed to be a plane monochromatic wave of the form

$$E_0 = A_0 \exp(i\mathbf{k}_0 \cdot \mathbf{r} - i\omega_0 t), \tag{2.9}$$

where $\mathbf{k}_0$ is the propagation vector of the incident light, and ω_0 is its angular frequency. Since E_0 satisfies (2.8a), we obtain the relation $k_0 = (\epsilon_0)^{1/2} \cdot (\omega_0/c)$

E_1 in equation (2.8b) can be solved for by double Fourier transformation in space and time. When R, the distance from the origin to the point of observation, is much larger than the largest dimension of the scattering medium, the space-time Fourier transform of $E_1(K,\omega_f)$ is given by[18]

$$E_1(K,\omega_f) = -\frac{A_0}{R} \cdot \frac{\sin\phi}{8c^2\pi^2} \cdot \exp(ik_f R) \int_{-\infty}^{+\infty} dt \, [\exp(i\omega_f t)]$$

$$\times \int_v dr^3 [\exp(i\mathbf{K}\cdot\mathbf{r})] \frac{\partial^2}{\partial t^2} \left[\Delta\epsilon(\mathbf{r},t)\exp(-i\omega_0 t) \right], \tag{2.10a}$$

or

$$E_1(K, t) = -\frac{A_0}{R} \cdot \frac{\sin\phi}{4c^2\pi} \cdot \exp(ik_f R)$$

$$\times \int_v dr^3 [\exp(i\mathbf{K}\cdot\mathbf{r})] \frac{\partial^2}{\partial t^2} \left[\Delta\epsilon(\mathbf{r},t)\exp(-i\omega_0 t) \right], \tag{2.10b}$$

where the space integration is over the volume of the scattering medium, $\mathbf{K} = \mathbf{k}_0 - \mathbf{k}_f$ is the difference between the wave vectors of incident and scattered light, ϕ is the angle between the electric vector of the incident wave $\mathbf{E}_0$ and the propagation vector of the scattered wave $\mathbf{k}_f$, and ω_f is the angular frequency of the scattered wave (Fig. 2.1). In practice the variation of $\Delta\varepsilon(\mathbf{r},t)$, which is caused by fluctuations in the medium, is much slower compared to the frequency of the incident light (about 10^{14}Hz). Its derivatives with respect to time can consequently be ignored compared to the time derivatives of the incident field, and (2.10b) becomes

$$E_1(K,t) = \frac{A_0}{R} \cdot \frac{\sin\phi}{4c^2\pi} \cdot \omega_0^2 \cdot \exp(ik_f R)$$

$$\times \int_V dr^3 \Delta\varepsilon(r,t)[\exp(iK\cdot r)] \qquad (2.11)$$

The intensity of the scattered light can be defined by the relation[19],

$$I(K,\omega_f,t) = \frac{1}{2\pi} \int \langle E_1(K,t)\cdot E_1^*(K,t'+t)\rangle \exp(i\omega_f t')dt', \quad (2.12)$$

where the angular brackets denote the average with respect to a stationary equilibrium ensemble. E_1^* is the conjugate of E_1. We also note from the properties of the canonical ensemble, that the ensemble average of a dynamical variable actually does not depend

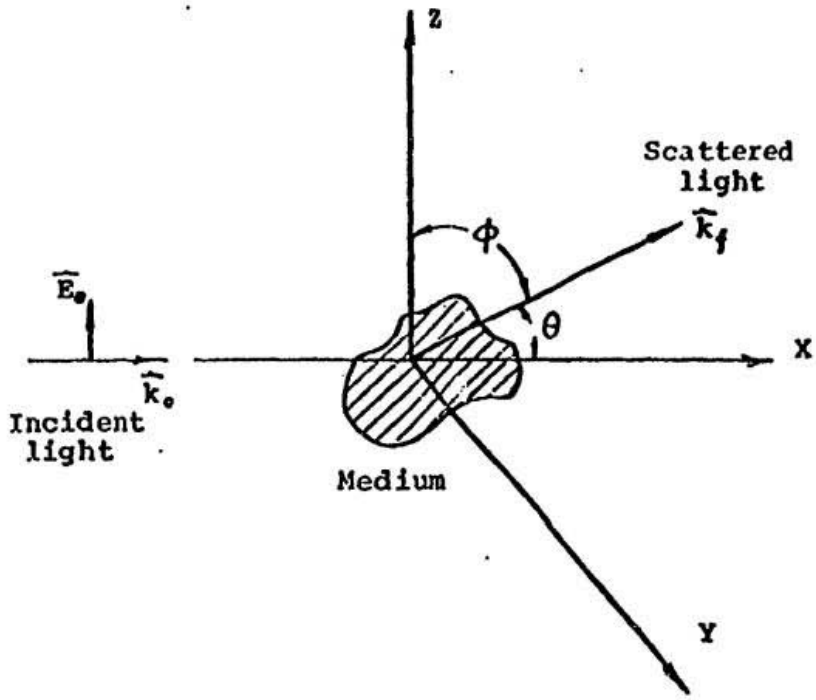

Fig. 2.1 The angles used in (2.10) are defined here. The electric field in the incident beam is along the z direction, and the incident beam propagates in the x direction. ϕ and θ are the angles between the propagation direction of the scattered beam and the z and x axes respectively.

on t, that is,

$$I(K,\omega_s) = I(K,\omega_s,0) = I(K,\omega_s,t). \tag{2.13}$$

Using the result (2.11), (2.12) and (2.13), we thus obtain the frequency distribution of the scattered light as

$$I(K,\omega_s) = \frac{|A_0|^2}{R^2} \cdot \frac{\sin^2\phi}{32\pi^2 c^4} \cdot \omega_0^4$$

$$\times \int_{-\infty}^{+\infty}\iiint \left[<\Delta\epsilon^*(r',0)\Delta\epsilon(r'',t)>\right] \cdot \exp[iK\cdot(r'-r'')+i(\omega_s-\omega_0)t]d^3r'd^3r''dt$$

$$\propto \int_{-\infty}^{+\infty}\left[<\epsilon^*(K,0)\epsilon(K,t)>\right]\exp[i(\omega_s-\omega_0)t]dt \tag{2.14}$$

Considering a binary mixture which is composed of N_1 molecules of species 1 and N_2 molecules of species 2 in volume V (if N_2=0, we can easily obtain the result for a simple fluid), the average partial number densities are $n_0^1=N_1/V$, $n_0^2=N_2/V$ and the total number of molecules is $N=N_1+N_2$. Let r_i^1 and r_i^2 denote the positions of molecule number i of species 1 and 2, respectively. Then the dielectric constant can be expanded in a Taylor series in the local density about the average density n_0^i (i=1,2) so that $\Delta\epsilon$ in (2.3) becomes

$$\Delta\epsilon(r',t) = \left[\frac{\partial\epsilon}{\partial n^1}\right]_{n^1=n_0^1}\cdot\Delta n^1 + \left[\frac{\partial\epsilon}{\partial n^2}\right]_{n^2=n_0^2}\cdot\Delta n^2 + \cdots$$

$$= \left[\frac{\partial\epsilon}{\partial n^1}\right]_{n^1=n_0^1}\cdot\left\{\sum_i\delta[r'-r_i^1(t)]-n_0^1\right\}$$

$$+ \left[\frac{\partial \varepsilon}{\partial n^2}\right]_{n^2=n_0^2} \cdot \left\{ \sum_j \delta[r' - r_j^2(t)] - n_0^2 \right\} + \cdots \qquad (2.15)$$

where $i = 1,2,\cdots,N_1$; $j = 1,2,\cdots,N_2$.

By substitution of (2.15) into (2.14), we obtain

$$I(K,\omega_f) \propto \int_{-\infty}^{\infty} dt \exp[i(\omega_f - \omega_0)t] \int d^3r' \int d^3r'' \exp[iK\cdot(r'-r'')]$$

$$\times \left\{ < \left[\frac{\partial \varepsilon}{\partial n^1}\right]_{n_0^1}^2 \left\{ \sum_i \delta[r' - r_i^1(t)] - n_0^1 \right\} \left\{ \sum_i \delta[r'' - r_i^1(t)] - n_0^1 \right\} >$$

$$+ < \left[\frac{\partial \varepsilon}{\partial n^2}\right]_{n_0^2}^2 \left\{ \sum_j \delta[r' - r_i^2(t)] - n_0^2 \right\} \left\{ \sum_j \delta[r'' - r_j^2(t)] - n_0^2 \right\} >$$

$$+ < \left[\frac{\partial \varepsilon}{\partial n^1}\right]_{n_0^1} \left[\frac{\partial \varepsilon}{\partial n^2}\right]_{n_0^2} \left\{ \sum_i \delta[r' - r_i^1(t)] - n_0^1 \right\} \left\{ \sum_j \delta[r'' - r_j^2(t)] - n_0^2 \right\} >$$

$$+ < \left[\frac{\partial \varepsilon}{\partial n^1}\right]_{n_0^1} \left[\frac{\partial \varepsilon}{\partial n^2}\right]_{n_0^2} \left\{ \sum_i \delta[r'' - r_i^1(t)] - n_0^1 \right\} \left\{ \sum_j \delta[r' - r_j^2(t)] - n_0^2 \right\} > \Big\}.$$

$\cdots\cdots(2.16)$

After further simplification (2.16) can be written as

$$I(K,\omega) \propto N_1\alpha_1^2 S_{11}(K,\omega) + N_2\alpha_2^2 S_{22}(K,\omega) + (N_1N_2)^{1/2}\alpha_1\alpha_2 S_{12}(K,\omega) + (N_1N_2)^{1/2}\alpha_1\alpha_2 S_{21}(K,\omega) \qquad (2.17)$$

where $\omega = \omega_f - \omega_0$, and α_i (which is proportional to $(\partial\varepsilon/\partial n^i)_{n^i=n_0^i}$ [19]) is the polarizability of species i. The $S_{ij}(i,j = 1,2)$, which are usually called the "partial dynamic structure factors", are defined by:

$$S_{ij}(K,\omega) = \frac{1}{2\pi}\int_{-\infty}^{+\infty} dt\ [\exp(i\omega t)]$$

$$\times\int d^3r'\int d^3r''\ \exp[iK\cdot(r'-r'')]<\delta\hat{n}_i(r',0)\delta\hat{n}_j(r'',t)>, \qquad (2.18)$$

where

$$\delta\hat{n}_i = \frac{1}{(N_i)^{1/2}}\cdot\left[\sum_i \delta(r-r_i(t)) - n_0^i\right]. \qquad (2.19)$$

Since for classical fluids in equilibrium all the $S_{ij}(K,\omega)$ are real, and are even functions of ω, we have

$$S_{ij}(K,\omega) = S_{ji}(K,\omega),\ (i,j = 1,2) \qquad (2.20)$$

and assuming the dilute fluid is isotropic, $S_{ij}(K,\omega)$ depends only on $K=|K|$. So all partial dynamic structure factors also satisfy

$$S_{ij}(K,\omega) = S_{ij}(K,\omega).\ (i,j = 1,2) \qquad (2.21)$$

Using (2.20) and (2.21) we can easily see (2.17) is just (1.3) used in Chapter 1.

It is clearly shown in (2.17) that the intensity of scattered light for binary fluids is proportional to the weighted sum of the partial dynamic structure factors given by the space-time Fourier transform of the density correlation functions. From the definition of dynamic structure factor (2.18) we can also see that S_{11}(or S_{22}) is only related to the microscopic properties

of the lighter(or the heavier) species in a binary mixture while the cross term S_{12} is related to the both. Most of the theoretical studies concerning thermal light scattering concentrate on using different methods to calculate the partial dynamic structure factors, thereafter the theoretical results can be compared with experiment. As was mentioned in Chapter 1, in the limit where $K\ell \ll 1$ the density fluctuations in a fluid are governed by hydrodynamic theory, while for the case where $K\ell \simeq 1$, on the other hand, kinetic theory is necessary. In the following two sections we will show how the partial dynamic structure factors are obtained in these two different regimes.

§. 2.2. HYDRODYNAMIC THEORY

In the hydrodynamic description, the fluctuations of the local dielectric constant are related to the fluctuations of a complete set of local thermodynamic quantities a_i such as pressure, temperature and concentration, i.e.

$$\Delta\epsilon(\mathbf{r},t) = \sum_i \left[\frac{\partial\epsilon}{\partial a_i}\right]_{a\neq a_i} \delta a_i$$

$$= \left[\frac{\partial\epsilon}{\partial p}\right]_{T,c} \delta p(\mathbf{r},t) + \left[\frac{\partial\epsilon}{\partial T}\right]_{p,c} \delta T(\mathbf{r},t)$$

$$+ \left[\frac{\partial\epsilon}{\partial c}\right]_{T,p} \delta c(\mathbf{r},t) \qquad (2.22)$$

Any three independent variables will suffice for binary fluids, but certain choices of variables may provide more convenience for the calculation than others[20].

The space and time response of the system to a deviation from equilibrium is calculated by using the linearized hydrodynamic equations and initial values for correlation functions provided by thermodynamic fluctuation theory. If (T,p,c) are chosen, then these equations are the continuity equation,

$$\left[\frac{\partial \rho}{\partial t} \right] + \rho_0 \nabla \cdot \mathbf{v} = 0, \tag{2.23}$$

the longitudinal part of the Navier-Stokes equation,

$$\rho_0 \left[\frac{\partial \mathbf{v}}{\partial t} \right] = -\nabla p + \eta_s \nabla^2 \mathbf{v} + (\tfrac{1}{3}\eta_s + \eta_v) \nabla (\nabla \cdot \mathbf{v}), \tag{2.24}$$

the diffusion equation,

$$\frac{\partial c}{\partial t} = D[\nabla^2 c + (k_T/T_0)\nabla^2 T + (k_p/p_0)\nabla^2 p], \tag{2.25}$$

and the energy transport equation,

$$\rho_0 C_p \cdot \frac{\partial T}{\partial t} - \rho_0 k_T \left[\frac{\partial \mu}{\partial c} \right]_{p,T} \cdot \frac{\partial c}{\partial t} + \rho_0 T_0 \left[\frac{\partial S}{\partial p} \right]_{T,c} \cdot \frac{\partial p}{\partial t} = \kappa \nabla^2 T \tag{2.26}$$

In these equations, all the equilibrium values are denoted by a subscript zero. ρ is the density, $\mathbf{v}$ is the mass velocity, μ is the

chemical potential of the mixture[21], η_s and η_v are the shear and volume viscosities respectively, D is the diffusion coefficient, S is the entropy, κ is the thermal conductivity, k_T is the thermal diffusion ratio, and k_p is a thermodynamic quantity defined by

$$k_p = - \frac{(p_0/\rho_0)(\partial\rho/\partial c)_{p,T}}{(\partial\mu/\partial c)_{p,T}}$$

Hence if we rewrite equations (2.23)-(2.26) in terms of the spatial Fourier transforms, we can obtain p(K,t), T(K,t) and c(K,t) in terms of initial fluctuations p(K), T(K) and c(K). Meanwhile the spatial Fourier transform of the local dielectric constant can be expressed as

$$\epsilon(K,t) = \left[\frac{\partial\epsilon}{\partial p} \right]_{c,T} p(K,t) + \left[\frac{\partial\epsilon}{\partial T} \right]_{p,c} T(K,t) + \left[\frac{\partial\epsilon}{\partial c} \right]_{T,p} c(K,t) \quad (2.27)$$

Using (2.27) and (2.14), the final expression can be obtained in the form

$$S(K,\omega) = \frac{A_{D1}}{z_{D1}^2 + \omega^2} + \frac{A_{D2}}{z_{D2}^2 + \omega^2} + \frac{A_B}{z_B^2 + (\omega - \omega_B)^2} + \frac{A_B}{z_B^2 + (\omega + \omega_B)^2} \quad (2.28)$$

where A_{D1}, A_{D2}, A_B, z_{D1}, z_{D2}, z_B and ω_B are coefficients depending on K. The Rayleigh peak cannot simply be considered as the superposition of the first two Lorentzians shown in (2.28). In fact, as the result of the coupling effects between diffusion and heat flow in a binary fluid, the actual central peak is the resultant of a much more complicated superposition which consists

of six Lorentzians(see ref. 20 for more detail).

In the hydrodynamic description the local equilibrium assumption is used, which means that at each point in a fluid the same thermodynamic relations can be used to relate different thermodynamic variables, and the fluid is considered to behave like a continuum. So the hydrodynamic theory is proper only for small K and ω under this condition, and the microscopic detail of local structure can be ignored.

§. 2.3. KINETIC THEORY & PREDICTION OF A FAST-SOUND MODE IN DISPARATE-MASS MIXTURES

In a dilute fluid where $K\ell \simeq 1$, hydrodynamic theory ceases to be an applicable theory. Kinetic theory, which involves a more detailed microscopic description, is needed. As will be seen later, kinetic theory is more general and includes hydrodynamic theory as a specific case. In this section, using kinetic theory, the dynamic structure factor for simple fluid is deduced.

Kinetic theory is based on the Boltzmann equation which involves the distribution function $f(\mathbf{r},\mathbf{v},t)$. In a fluid this distribution function is defined in such way that $f(\mathbf{r},\mathbf{v},t)\Delta\mathbf{r}\Delta\mathbf{v}$ is the average number of particles at time t inside the volume $\Delta\mathbf{r}$ around position $\mathbf{r}$, and with velocities within the range $\Delta\mathbf{v}$ around

v. Because the intermolecular interaction range is much smaller than the average intermolecular distance in a dilute fluid, it is unlikely that more than two particles will collide at the same time. Therefore under the molecular-chaos assumption the Boltzmann equation (2.29) gives us the time evolution of $f(\mathbf{r},\mathbf{v},t)$:

$$\frac{\partial}{\partial t}f(\mathbf{r},\mathbf{v},t)+\mathbf{v}\cdot\nabla f(\mathbf{r},\mathbf{v},t)-\int d^3v\int d\Omega \cdot \sigma(\theta,|\mathbf{v}-\boldsymbol{v}|)\cdot|\mathbf{v}-\boldsymbol{v}| \times [f(\mathbf{r},\mathbf{v}',t)f(\mathbf{r},\boldsymbol{v}',t) - f(\mathbf{r},\mathbf{v},t)f(\mathbf{r},\boldsymbol{v},t)] \qquad (2.29)$$

where $\mathbf{v}'$ and $\boldsymbol{v}'$ (which are the velocities of two particles, after a binary collision, with initial velocities $\mathbf{v}$ and $\boldsymbol{v}$, respectively) depend on their initial velocities and the scattering angle (θ,ϕ) in polar coordinates (polar axis parallel to $\mathbf{v}-\boldsymbol{v}$). Ω in (2.29) is the solid angle and $\sigma(\theta,|\mathbf{v}-\boldsymbol{v}|)$ is the differential collision cross section.

The most important result of the Boltzmann equation is that for any given initial distribution function, $f(\mathbf{r},\mathbf{v},t_0)$, the solution of (2.29) will approach the absolute equilibrium Maxwell distribution function:

$$f(\mathbf{r},\mathbf{v},t) \to f_M(\mathbf{v}) = n\left(\frac{\beta m}{2\pi}\right)^{3/2}\exp(-\beta m\mathbf{v}^2/2) \qquad (2.30)$$

where n is the average number density of the fluid. This result is also known as "Boltzmann's H-theorem". The assumption which follows is that equation (2.29) can be linearized because the distribution function $f(\mathbf{r},\mathbf{v},t)$ is close to its equilibrium form, $f_M(\mathbf{v})$. If we

define a small perturbation of the distribution function as $\Delta f(\mathbf{r},\mathbf{v},t)$, then $f(\mathbf{v},\mathbf{r},t) = \Delta f(\mathbf{v},\mathbf{r},t) + f_M(\mathbf{v})$. Substitution of the latter form into (2.29), while considering only the first order of Δf, yields the linearized equation for $\Delta f(\mathbf{r},\mathbf{v},t)$;

$$\frac{\partial}{\partial t}[\Delta f(\mathbf{r},\mathbf{v},t)] + \mathbf{v}\cdot\nabla[\Delta f(\mathbf{r},\mathbf{v},t)] = \Lambda_B[\Delta f(\mathbf{r},\mathbf{v},t)], \qquad (2.31)$$

where Λ_B is a linear integral operator which acts only on $\mathbf{v}$.

Now we introduce the dynamic variable $\hat{f}(\mathbf{r},\mathbf{v},t)$ which is given by

$$\hat{f}(\mathbf{r},\mathbf{v},t) = \sum_{p=1}^{N}\delta[\mathbf{r}-\mathbf{r}_p(t)]\delta[\mathbf{v}-\mathbf{v}_p(t)]. \qquad (2.32)$$

It can be seen that $\hat{f}(\mathbf{r},\mathbf{v},t)$ describes the particles' position and velocity distribution at time t, and that its ensemble average is just equal to the equilibrium distribution function $f_M(\mathbf{v})$, while its perturbation $\Delta\hat{f}(\mathbf{r},\mathbf{v},t) = \hat{f}(\mathbf{r},\mathbf{v},t) - f_M(\mathbf{v})$ satisfies the equation (2.31). According to the Onsager regression hypothesis in statistical mechanics[19], the decay of microscopic spontaneous fluctuations of a dynamic variable, and the decay of its correlation function, on the average, follow the same linearized equation. Therefore we can replace $\Delta f(\mathbf{r},\mathbf{v},t)$ in (2.31) with the correlation function

$$C(|\mathbf{r}-\mathbf{r}'|,\mathbf{v},\mathbf{v}',t) = V\langle\Delta\hat{f}(\mathbf{r},\mathbf{v},t)\Delta\hat{f}(\mathbf{r}',\mathbf{v}',0)\rangle, \qquad (2.33)$$

and obtain

$$\frac{\partial}{\partial t}C(|r-r'|,v,\ v',t) + v\cdot\nabla C(|r-r'|,v,\ v',t)$$

$$= \Lambda_B C(|r-r'|,v,\ v',t). \qquad (2.34)$$

Because of the isotropic condition in dilute fluids, the correlation function in (2.33) depends only on the modulus of the relative position, and the factor V introduced there is for calculation convenience. Then the spatial Fourier transform of (2.33) can be written as

$$C(K,v,v',t) = \int d^3|r-r'|\ \exp[-iK\cdot(r-r')]C(|r-r'|,v,v',t)$$

$$= \int d^3|r-r'|\ d^3r\ <\Delta\hat{f}(r,v,t)\Delta\hat{f}(r',v',0)>\exp[-iK\cdot(r-r')]$$

$$= <\Delta\hat{f}^*(K,v,t)\Delta\hat{f}(K,v',0)>, \qquad (2.35)$$

where

$$\Delta\hat{f}(K,v,t) = \sum_{p=1}^{N} \delta[v-v_p(t)]\exp[-iK\cdot r_p(t)]. \qquad (2.36)$$

and because of isotropy at equilibrium, $C(K,v,v',t)$ depends on $K = |K|$. The equation for $C(K,v,v',t)$ is obtained from the Fourier transform of equation (2.34)

$$\frac{\partial}{\partial t}\ C(K,v,v',t) + iK\cdot vC(K,v,v',t) = B(K)C(K,v,v',t), \qquad (2.37)$$

where $B(K)$ is a linear integral operator. Using (2.18), (2.19) (considering components i,j are the same), (2.32), and (2.33) the stucture factor can immediately be obtained as

$$S(K,\omega) = \frac{1}{2\pi N}\int dt\ \exp(i\omega t)\left[\int d^3v d^3v' C(K,v,v',t)\right], \quad (2.38)$$

so the key problem remaining is to find a way of calculating $C(K,v,v',t)$.

Since the Boltzmann equation is valid only in the limit of dilute gases, based on a hard-sphere model Cohen and Campa used a modified Enskog theory in order to obtain the more general results which are valid for both dilute and dense fluids. And instead of trying to obtain $C(K,v,v',t)$ directly from the equation similar to (2.37) which proved to be quite difficult, they attempted an indirect way by calculating an infinite set of correlation functions[22,23]. The computations of partial structure factors $S_{ij}(K,\omega)$ are performed by a spectral decomposition of a time-evolution operator $L_\Sigma(K)$ in terms of discrete eigenmodes. The final result for the partial structure factor can be expressed as a sum of Lorentzians:

$$S_{ij}(K,\omega) = \mathrm{Re}\sum_{N}\frac{A_{ij,n}(K)}{i\omega - z_n(K)}\ , \quad (2.39)$$

where the sum runs over the eigenvalues $z_n(K)$ of $L_\Sigma(K)$, and $i,j = 1,2$ denote two different components of the mixture, $A_{ij,n}(K)$ are the amplitudes corresponding to the eigenvalue $z_n(K)$, N is the number of eigenvalues used, which is chosen on the basis of the Bhatnagar-Gross-Krook method[23]. These different eigenmodes can be interpreted as the different channels by which the fluctuations decay in time.

In Campa's calculation the eigenvalues of the kinetic operator $L_{\xi}(K)$ fall into two types. One type is real and another is complex. Because of the existence of damping processes, the real parts of both types are negative. The complex eigenvalues always come in conjugate pairs and their real parts represent damping processes while imaginary parts represent propagation processes in two opposite directions.

In the hydrodynamic limit, (i.e. for K of sufficient small value) all the amplitudes $A_{ij,n}(K)$ are real and contributions to the sum (2.39) come only from four eigenmodes with following eigenvalues

$$z_{1,2}(K) = \pm ic_s K - \Gamma K^2, \tag{2.40a}$$

and

$$z_3(K) = -D_1 K^2, \tag{2.40b}$$

$$z_4(K) = -D_2 K^2, \tag{2.40c}$$

where c_s is the adiabatic velocity of sound which is independent of K, and D_1, D_2, Γ are positive coefficients associated with the damping process. Therefore for $K \to 0$, substitution of (2.40) into (2.39) shows that the kinetic result is in agreement with hydrodynamic result (2.28). The description in terms of discrete modes is thus a generalization of the hydrodynamic theory.

When the conditions are beyond the hydrodynamic regime, the situation becomes more complicated. Contributions from higher propagating modes must be taken into account, and some of the amplitudes $A_{ij,n}(K)$ can be complex. The eigenvalues for diffusive modes are still real, but the eigenvalues of the propagating modes come in complex conjugate pairs and eigenvalues should be written in the general form

$$z_n = i\omega_n(K)+\gamma_n(K) \tag{2.41}$$

where the negative real part $\gamma_n(K)$ represents the damping, and the imaginary part $\omega_n(K)$, which is the dispersion relation for the n-th mode, determines the propagation velocity of the mode assoicated with $z_n(K)$ (the group velocity of the n-th mode c_s is given by $d\omega_n(K)/dK$). Contrary to the hydrodynamic limit, $\omega(K)$ can no longer be expressed in simple form as the product of K and c_s which is independent of K.

In the calculation for dilute, disparate-mass, binary mixtures of $Ar+H_2$, Campa found that under the conditions of high concentration of the lighter component and K larger than a certain value, one of the eigenvalues he obtained had an imaginary part $\omega_n(K)$ for which the group velocity $d\omega(K)/dK$ was considerably larger than that of other modes. Calculation of the partial dynamic structure factors showed that this fast mode was only associated with the light component and would give an observable

shoulder or peak only in the partial dynamic structure factor $S_{11}(K,\omega)$. No shoulder or peak would appear in $S_{12}(K,\omega)$ and $S_{22}(K,\omega)$. This shoulder or peak in $S_{11}(K,\omega)$ leads, for a proper choice of the two components (the combination of $Ar+H_2$ was suggested by Campa), to a shoulder in the differential cross section for Brillouin scattering. This implies that the fast mode is associated only with the light component.

Chapter 3. Apparatus and Experimental Procedure

The overall arrangement of apparatus used to study Brillouin scattering from the gas mixtures is schematically depicted in Fig. 3.1. An Ar^+ laser was used as the incident light source. The spectrometer consisted of a piezoelectrically-scanned Fabry-Perot interferometer, a photomultiplier tube and a Data Acquisition and Stablization System (DAS-1). The spectral data were first accumulated for several hours in the DAS memory and then transmitted to a personal computer for further processing. More detail is given in following sections.

§. 3.1. OPTICAL SYSTEM

Because the frequency shifts observed in Brillouin scattering are very small (less than 10GHz in our experiment), the incident radiation must be highly monochromatic. The exciting radiation used in our experiment was provided by an Ar^+ laser (Coherent

Fig. 3.1 Schematic diagram of the experimental setup.

C sample cell;

BS beam-splitter;

AT partially penetrating glass attenuater;

S electromechanical shutter;

MP microprocessor;

GF glass fiber;

F narrow-band grating filter;

F-P Fabry-Perot interferometer;

PH pinhole;

PM thermoelectrically-cooled photomultiplier;

DAS data acquisition and stablization system;

M1, M2, M3, M5, and M6 mirrors;

M4 uncoated reflector;

AP1 and AP2 apertures;

L1, L2, L3, and L4 lenses.

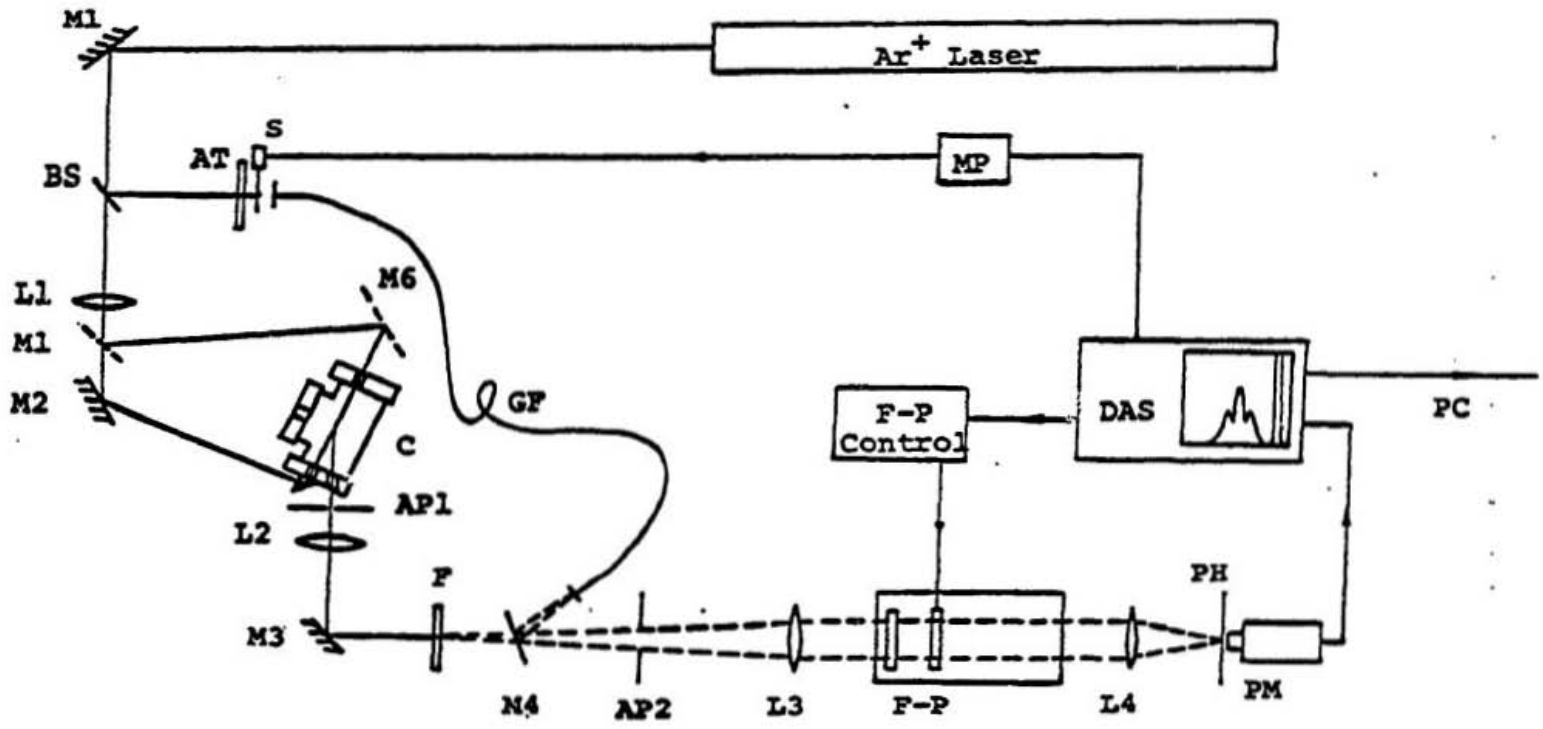
M1
Ar+ Laser
S
AT
MP
BS
L1
M6
M1
M2
GF
C
F-P
Control
DAS
PC
AP1
L2
F
PH
M3
M4
AP2
L3
F-P
L4
PM

Radiation, Model Innova 90-5) which was operated in a single cavity mode with a nominal wavelength of 514.5nm and output power of 300-500mW. Selection of the output light frequency was made possible by using an intracavity prism. An intracavity etalon was installed inside the resonator for obtaining a narrow laser linewidth. The tilt of the etalon could be adjusted to obtain a single mode. After several hours warm-up, both the frequency and power output of the laser was generally quite stable. No further attempt was made for laser stabilization in this experiment.

Since light scattering experiments at low or moderate pressure (less than 10 atm. in our experiment) involved measurements of light at very low intensity levels, long data aquisition times (from 5 to 24 hours) were required. In order to minimize the effects of long term drift in the interferometer alignment, it was consequently necessary to utilize the feedback control capability of the DAS-1 where a reference laser signal was provided as follows: The laser beam was first divided into two parts by using a beamsplitter (BS), of uncoated glass. Then the reflected light was attenuated and transmitted through an optical glass-fiber (GF) when the shutter (S) was open. The output of glass-fiber was accurately directed along the optical axis of spectrometer by a second uncoated reflector (M4), and finally collected in the DAS-1 for feedback control(see section 3.2).

The main laser beam was focused by lens L1, and then

reflected by mirror M2 and a prism into the center of scattering cell C. The scattering angle formed by the incident beam and the scattered light was about 157.5°. This configuration also permitted us to observe the spectrum corresponding to a smaller scattering angle of 22.5° by adding two mirrors M5, M6 as shown in Fig. 3.1, while keeping the distance from L1 to the centre of the cell almost unchanged. The scattered light passing through aperture AP1 was collected by the lens L2 and focused at a point which was just coincident with the virtual image of the bright head of the glass-fiber produced by M4. Mirror M3 was used to direct the scattering light to a Fabry-Perot (FP) interferometer (Burleigh, Model RC-110). F was an adjustable narrow-band monochromatic grating filter (KRATOS, Model GM 100-2), which was adjusted only to transmit the light signal near the wavelength 514.5nm and to reject unwanted Raman radiation from the samples. Because of the low intensity of the scattered light, it was necessary to minimize the intensity of the stray light. The apertures AP1 and AP2 were used to prevent unwanted stray light from getting into the spectrometer. This fact was also considered in the design of the scattering cell.

Aperture AP2, pinhole PH, lenses L3 and L4, the Fabry-Perot interferometer FP, the photomultiplier tube PM and a thermostatically controlled heater were all contained in a styrofoam box covered with black polyethylene. In addition, a large piece of heavy black cloth was draped over the box. The

purpose of this was first to exclude stray light and secondly to provide protection from temperature fluctuations of the surroundings so as to maintain the temperature inside the box around 20°C. A 4cm hole was cut in the styrofoam box so that the lens L3 could direct both the scattered light from cell and the reference laser signal to the Fabry-Perot interferometer.

In our experiments, the Fabry-Perot interferometer consisted of two flat mirrors (with flatnesses of $\lambda/200$ and reflection ratios of 98%) mounted parallel to each other in an adjustable super invar assembly. If the cavity between the mirrors is illuminated with a beam of monochromatic light, it will transmit the beam only when the relation (3.1) is satisfied, i.e.

$$m\lambda = 2nd\cos\theta \qquad (3.1)$$

where m is the order of interference, λ is wavelength of the incident light, n is the refractive index of medium between the two mirrors, d is the mirror spacing, and θ is the angle formed by the incident beam and the normal line of the plates (in the present experiments, $n \approx 1$, $\theta \approx 0$). The front mirror was mounted on an adjustable mount using three extremely fine differential micrometer adjustment assemblies. The rear mirror was supported by three stacks of piezoelectric transducers placed around its circumference. The spectrum of the scattered light was obtained by changing the voltage applied to the piezoelectric transducers,

which consequently changed the spacing between two plate mirrors. The fringes produced by the interference between the parallel mirrors were focused on a pinhole (PH) installed in front of the photomultiplier. The diameter of pinhole was important to the overall finesse of the spectrometer. If too large it broadened the line and if too small it cut down the transmitted intensity[24]. The appropriate size of the pinhole, which was generally selected by trial and error, ranged from 100μm to 200μm and the observed finesse was about 45. The photomultiplier tube (ITT Model, FW130) was mounted in a thermoeletrically-cooled, RF-shielded chamber, which maintained the cathode temperature at -20°C and reduced the dark count of the photomultiplier to about 1 count per second.

§. 3.2. DATA AQUISITION AND STABILIZATION SYSTEM (DAS-1)

The long experimental runs needed for low intensity spectra required high stability of both the interferometer and laser. However, changes of interferometer alignment and frequency drifting of the laser which could significantly broaden the instrumental linewidth are largely unavoidable, it was necessary to compensate for such drifting effects. This was made possible by using the DAS-1 in conjunction with a reference signal which was mentioned previously.

The master clock of the DAS-1 produces pulses which are used

to step the data accumulation through successive channels of a 1024 channel scaler. These pulses are themselves accumulated and subsequently converted through a DAC to produce the scanning ramp voltage which is applied simultaneously to all three of the piezoelectric transducers on which one of the Fabry-Perot mirrors is mounted. A single cycle in the repetitive scanning process was usually completed in less than 5 seconds, and the amplitude of the ramp was chosen to cover slightly more than two full orders of interference (i.e. so that three successive Rayleigh peaks could be observed). The highly linear relation between applied voltage and piezoelectric extension results in a corresponding relation between channel number and frequency (see Eq. 3.1 for θ=0). Compensation for instrumental drifts is made possible by the provision for external adjustment and control of the zero level of the voltage ramp. It is thus possible to select a reference peak in the observed spectrum and, through feedback control, force the peak to maintain its position at a preselected channel number. In the present case, however, the scattered light intensity was not sufficient for the purpose, and it was necessary to provide a reference signal of higher intensity through direct sampling of the laser beam.

The electromechanical shutter S was controlled by a separate microprocessor, MP, which utilized the digital clock of the DAS-1 as time base. It was programmed to open the shutter at a point (usually near the end of each sweep) where resonant transmission

at the laser frequency was about to occur, and to close it immediately after scanning the laser profile so that none of this high intensity signal could contaminate the (low intensity) Brillouin spectrum. Any tendency for this reference peak to drift away from its preselected location was detected by the DAS-1 when operating in its feedback control mode, and an appropriate adjustment to the zero level of the scanning ramp was automatically made to compensate for the drift. A similar but somewhat more complicated method is also provided for optimization of the instrumental finesse. Details of how the feedback controls are achieved can be found elsewhere[25,26].

Another important feature of DAS-1 is segmented scanning which permits different scanning speed for accumulating counts in the selected regions. In our experiments two segments were set for the DAS-1. The main segment for the spectrum we were interested in was set between channel numbers 310-730, and the laser segment, which was used to provide enough counts for the reference laser signal, was set between channel numbers 925-955. The speed ratio between the fast and slow portion of the ramp was 99, so that for each scan almost 90% of time was used in the main segment. The spectrum was accumulated in a total time of between 5 to 24 hours. A typical spectrum obtianed from the DAS-1 is shown in Fig. 3.2.

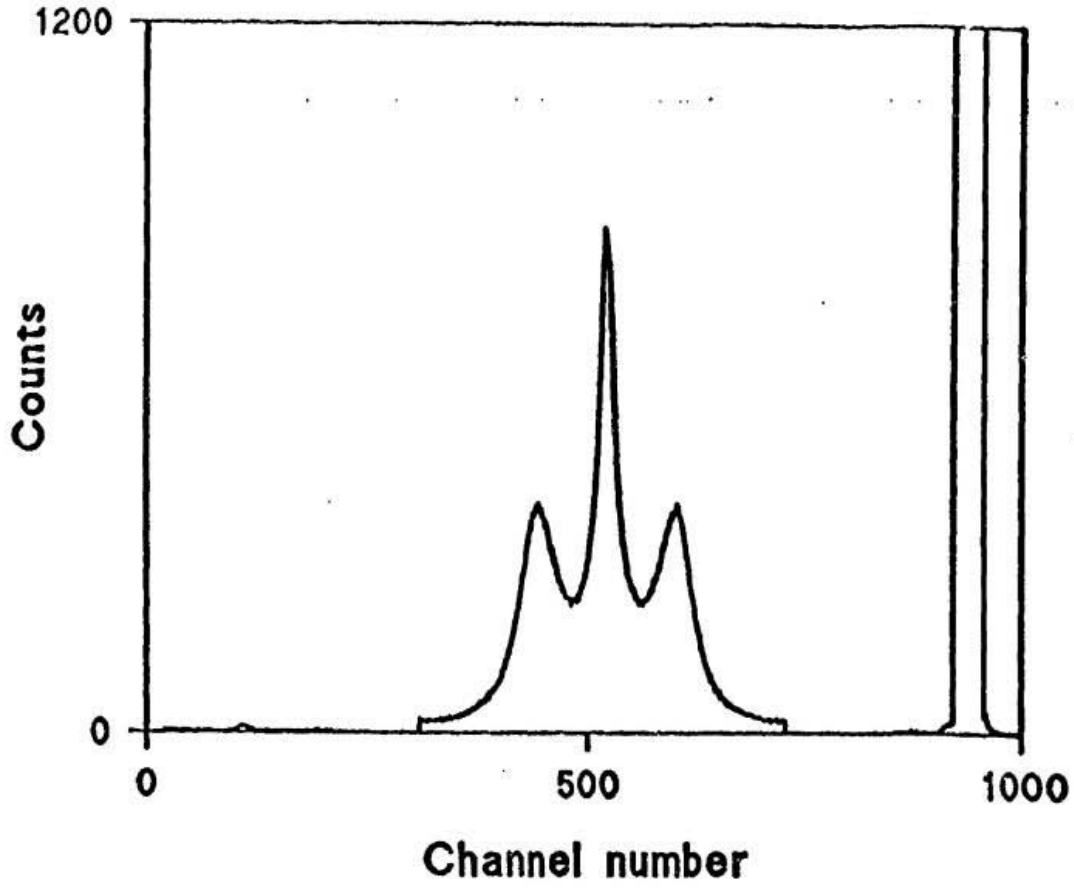

Fig. 3.2 Typical spectrum recorded in Brillouin scattering experiment (CH_4 + SF_6 mixture wich CH_4 base pressure of 6.3 bar and x_{SF_6}=0.08).

§. 3.3. GAS HANDLING SYSTEM

A block diagram of the gas handling system is shown in Fig. 3.3. The high purity (>99.99%) gases used in our experiments were provided by Matheson Gas Products. A Bourdon-tube gauge with an estimated accuracy of ±0.05 bar was used to measure the gas pressures.

The sample gases, for example SF_6 and CH_4, were mixed using the following procedures. Refering to Fig. 3.3, first we closed valves V3, V4, V5, V6, and V7, opened valves V1, V2, and V8, turned on the rotary vacuum pump. The scattering cell and the connected tubes could be evacuated to a pressure of about 10^{-2} torr. Then we closed valve V8, opened V4, and slowly filled the scattering cell with CH_4 in order to reduce the gas turbulence which could disturb any dust inside the cell. When the gauge reached the base pressure needed, we closed valves V1 and V4, opened V8, and turned on the rotary vacuum pump to evacuate the connecting tubes. The procedure followed was to close V8, open V3 and fill the connecting tubes with SF_6 until the reading on the gauge was a little bit higher than the pressure inside the cell, then close V3, opened V1 and added SF_6 into the cell. By repeating this process we obtained the gas mixtures of different partial pressure ratios. We needed to be careful during the whole process to keep the pressure inside the connecting tubes a little higher than the presure inside the cell.

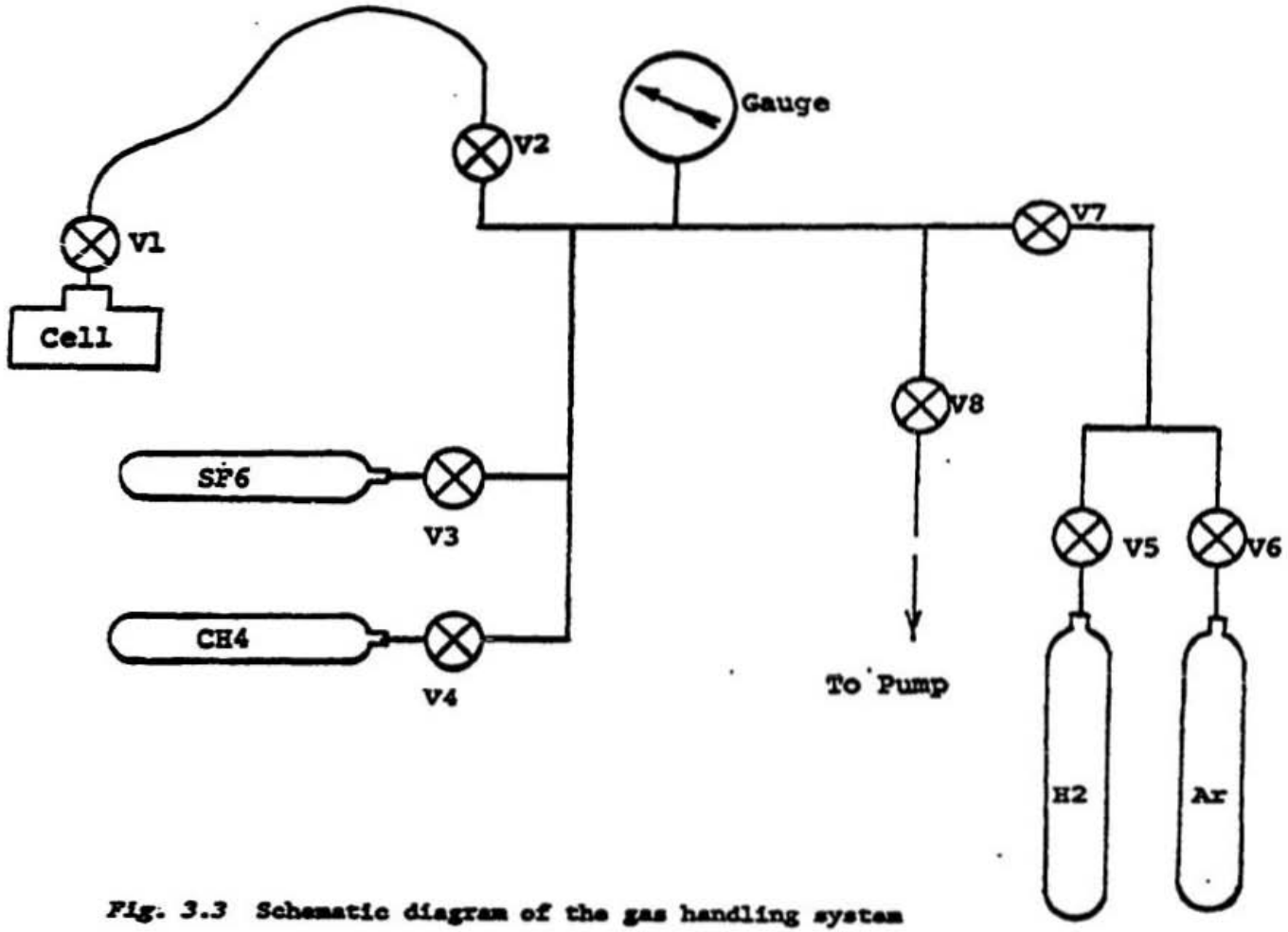

Fig. 3.3 Schematic diagram of the gas handling system

The entire experiment were performed in an air-conditioned room. No extra precautions were taken to keep the scattering cell at constant temperature.

Chapter 4. Experimental Results and Discussion

§. 4.1. GENERAL REMARKS

The method used to detect the fast or slow mode contribution to a given spectrum was to compare the observed sound velocity v_s' and the sound speed v_s calculated using the hydrodynamic theory ($K \to 0$). v_s' was determined by the Brillouin equation,

$$v_s' = \nu_B \lambda/[2\sin(\theta/2)], \qquad (4.1)$$

where ν_B is the observed frequency shift, λ is the wavelength of the incident light in the medium, and θ is the scattering angle. Initially, the law of partial pressures was assumed to be valid for all mixtures studied, and values of v_s were calculated via the ideal gas relation $v_s = (\gamma p/\rho)^{1/2}$, where $\gamma = c_p/c_v$, p is the pressure, and ρ is the mass density (for a given mixture). Subsequently more accurate values for v_s were obtained through collaboration with Dr. J. A. Zollweg of the School of Chemical

Engineering, Cornell University[27]. Zollweg's technique utilized the basic relation[28],

$$v_s = (V_m/M\kappa_s)^{1/2}, \qquad (4.2)$$

where V_m is the molar volume of the mixture, M is the average molecular weight, and κ_s is the adiabatic compressibility. Because the actual average molecular weight for a disparate-mass mixture could be significantly different from that calculated on the basis of partial pressures, the measured pressures were first used to calculate the concentration of each species via the virial state equation. Then the sound speed is obtained using the virial form

$$v_s^2 = (RT/M)\times\left[1+\frac{Bp}{RT}\right]\times\left\{1-R\left[1+\frac{p}{R}\frac{dB}{dT}\right]^2\times\left[C_p^0-pT\frac{d^2B}{dT^2}\right]^{-1}\right\}^{-1}, \qquad (4.3)$$

where p is again the total pressure, C_p^0 is the ideal-gas heat capacity, and B, the second virial coefficient for the mixture, is obtained by using Hayden-O'Connell method[29]. As it turned out, the values of v_s obtained by the second method were not significantly different from the initial calculations, with one or two exceptions.

§. 4.2. THE FAST SOUND MODE IN H_2 + Ar MIXTURES

A dilute gas mixture which is composed of two species with a

large mass difference responds to a thermal fluctuation with propagating density waves. Under conditions of high concentration of the lighter component, a density wave of high frequency and short wave length might only be supported by the lighter particles without the participation of the heavier particles in the collective motion. In this case the group velocity of the mixture is very close to the sound velocity in the single-component fluid which is obtained by removal of all heavier particles. The dynamics of the two components are thus partially separated. The contribution of the heavier component to the propagation mode is negligible because the heavier particles are unable to follow the fast sound mode which is caused by the rapid oscillations associated with the lighter component.

The wave vector K of the local density perturbation to be detected, corresponding to a scattering angle θ, satisfies the relation (1.1). So the length scale of the thermal fluctuation to be probed is given by $\Lambda = 2\pi/K = \lambda/[2\sin(\theta/2)]$, where λ is the wavelength of incident light in the medium. Because the fast sound mode, which corresponds to a short wavelength perturbation in the fluid, ceases to propagate if K is smaller than a certain value[23], a large scattering angle (157.5°) was selected in our experiments. For each series of experiments the sample cell was first charged with enough of the lighter species so that well-defined Brillouin peaks could be observed in the spectrum. This spectrum was subsequently monitored as successive increments of

the heavier species were added into the cell. Because of the fast sound mode effect, it was expected that the position of the Brillouin peak would remain substantially unchanged, or shift much less than expected on the basis of the hydrodynamic theory.

Three groups of spectra were collected for different H_2 base pressures. The mixtures, conditions are listed as follows:

$0 \le x_2 \le 0.23$, $0.21 \le K\ell_1 \le 0.27$, $K\ell_2 \simeq 0.07$, $p_1 = 9.0$ bars,

$0 \le x_2 \le 0.18$, $0.27 \le K\ell_1 \le 0.32$, $K\ell_2 \simeq 0.09$, $p_1 = 7.7$ bars,

$0 \le x_2 \le 0.17$, $0.33 \le K\ell_1 \le 0.39$, $K\ell_2 \simeq 0.10$, $p_1 = 6.3$ bars,

where x_i is the concentration of species i (1 and 2 refer to the light and heavy species, respectively) and ℓ_i is the mean free path of species i obtained using the conventional way which has been discussed in Chapter 1. The σ values that were used in the calculations were $\sigma_1 = 0.297$nm and $\sigma_2 = 0.340$nm for H_2 and Ar respectively. The contribution of the fast sound mode to the spectrum was observed in all three cases for low concentrations of Ar (Fig. 4.1-4.3). As the concentration of the heavy species increased, the Brillouin peaks were decidedly broadened due to the severe attenuation of sound. For $x_2 \ge 0.1$ the Brillouin peaks became unrecognizable. However, for $x_2 \le 0.1$, it is clear that the peak positions on the scale of normalized frequency shifts (the solid triangles) differ increasingly from positions (the open triangles) obtained using hydrodynamic theory ($K \to 0$) as the concentration of

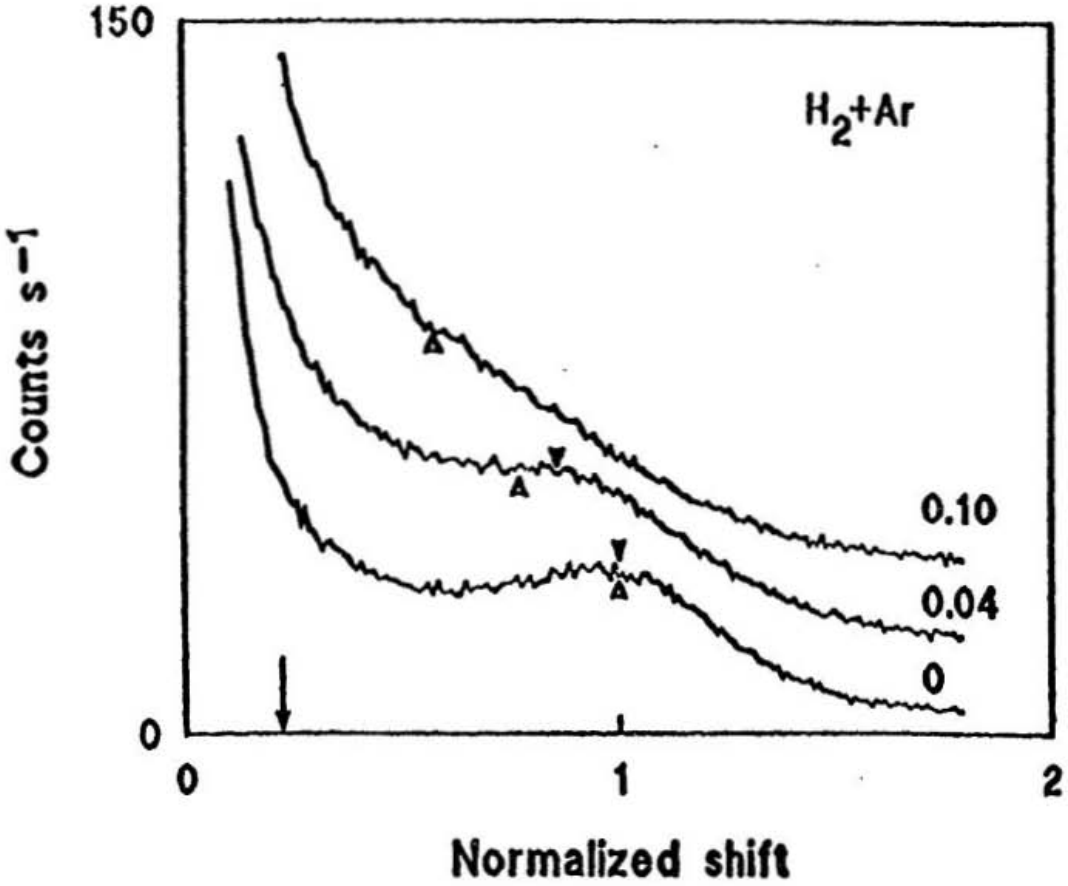

Fig. 4.1 Spectra for Ar+H_2 mixtures with a H_2 base pressure of 9.0 bars and fractional concentration of Ar as indicated. The central peaks have been removed to permit stacking of the spectra on an appropriate scale. The frequency shifts are normalized to unity at the position of the Brillouin peak for pure H_2 (each horizontal division corresponds to 9.2GHz). Only the (Stokes) region of down-shifted frequency is shown. The open triangles indicate the normalized shifts obtained based on hydrodynamic theory, while the solid triangles designate the estimated position of the observed Brillouin features, The arrow indicates the normalized position of the Brillouin peak for pure Ar. The scattering angle was 157.5°.

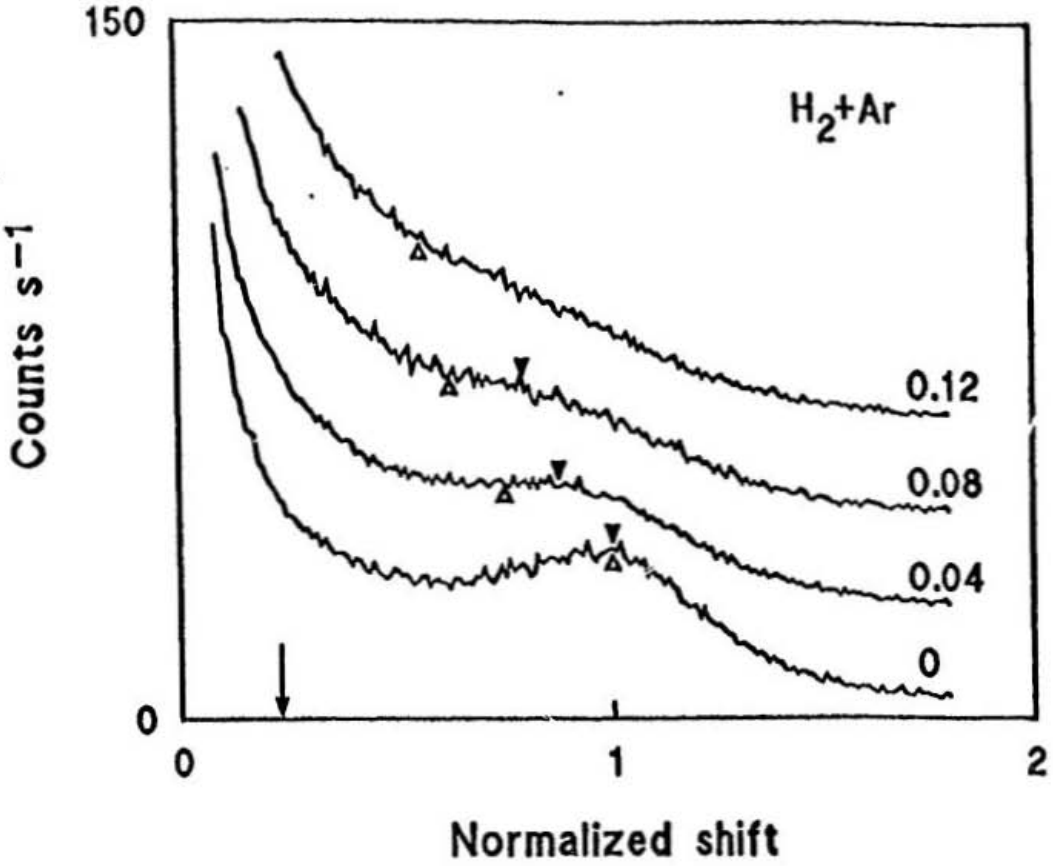

Fig. 4.2 Spectra for Ar+H_2 mixtures with a fixed H_2 pressure of 7.7 bars. See Fig. 4.1 for additional legend.

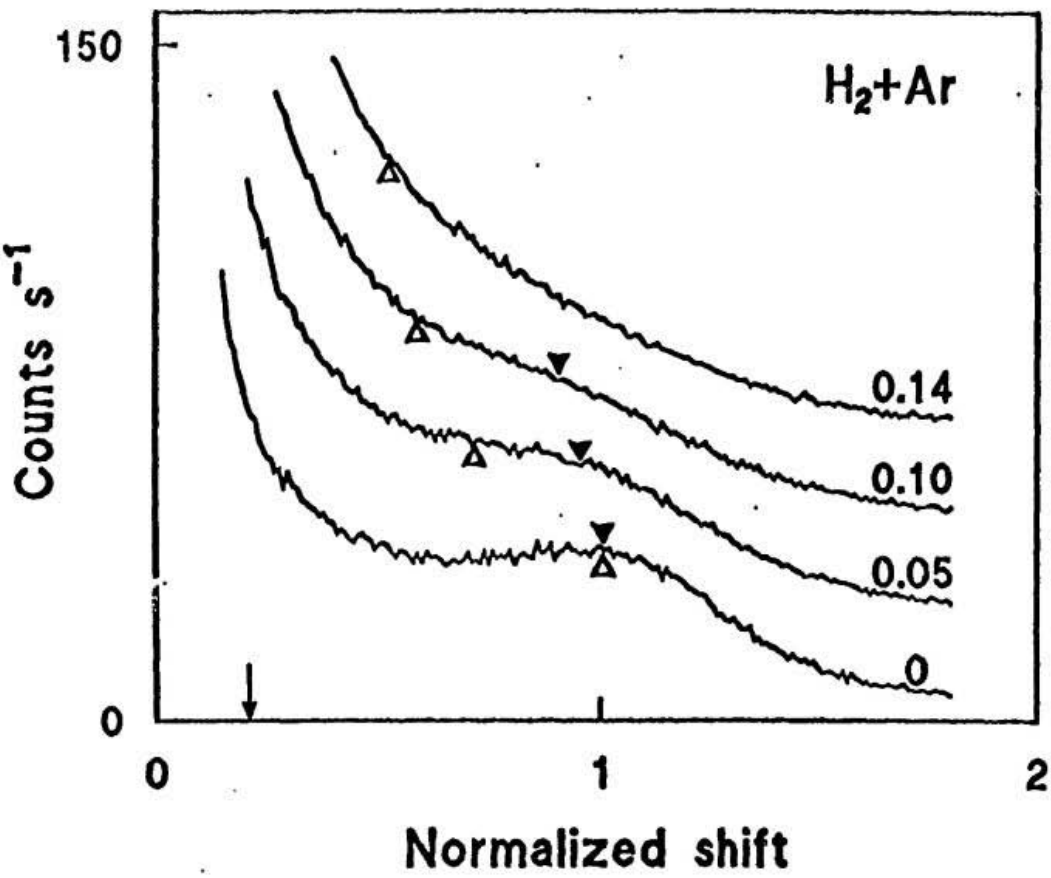

Fig. 4.3 Spectra for Ar+H_2 mixtures with a fixed H_2 pressure of 6.3 bars. See Fig. 4.1 for additional legend.

the heavy component is increased.

Based on our experimental results[30], Campa used the hard sphere model and performed calculations[31] to produce theoretical Brillouin spectra for Ar+H_2 mixtures with a H_2 base pressure of 6.3 bars. He found that the relative positions of the observed peaks, with respect to the peak positions calculated on the basis of hydrodynamics (the ratio of the solid triangle positions to the open triangle positions in Fig. 4.3), agreed with his calculated spectra (Table 4.2). He also found for x_2=0.14, as observed experimentally, that there is no visible contribution from the fast sound mode in the Brillouin spectrum.

Table 4.2 Comparison of the Present Experimental Results and Campa's Calculations for an Ar+H_2 Mixture with a H_2 Base Pressure of 6.3 bars

x_2	Observed Result	Campa's Calculation
0.05	1.30	1.20
0.10	1.51	1.46

As shown in Fig. 4.1-4.3, considerable difficulty was experienced in detecting the fast mode contribution as a well-defined spectral feature. This might be due to (i) a relatively high polarizability of Ar (α_{Ar}=1.64x10^{-24}/cm^3, α_{H_2}=0.82x10^{-24}/cm^3 $\alpha_{Ar}/\alpha_{H_2}\simeq 2$) which favors the second and third terms in (1.3),

(ii) broadening of the spectral feature because of the strong attenuation of the fast sound mode caused by the heavier particles, and (iii) the low absolute polarizability of H_2 which leads to a low signal level in the density range of interest. The relatively high intensity of the central peak also indicated that the data might be contaminated by stray light.

§. 4.3. CH_4 + SF_6 MIXTURES

Bearing the foregoing points in mind, mixtures of CH_4+SF_6 were selected for further investigations. The polarizability of CH_4 is about three times greater than that of H_2 ($\alpha_{CH_4}/\alpha_{H_2} \simeq 3.2$). In addition, the polarizability ratio of SF_6 and CH_4 is about the same as that of Ar and H_2 ($\alpha_{SF_6}/\alpha_{CH_4} \simeq 1.8$). However, the mass ratio for the new combination ($m_{SF_6}/m_{CH_4} \simeq 9.1$) is lowered roughly by a factor of 2. Two groups of spectra were collected for CH_4 base pressures of 6.3 bars and 3.7 bars, with conditions as follows:

$$0 \leq x_2 \leq 0.27,\ 0.17 \leq K\ell_1 \leq 0.23,\ K\ell_2 \simeq 0.07,\ p_1 = 6.3 \text{ bars},$$
$$0 \leq x_2 \leq 0.30,\ 0.28 \leq K\ell_1 \leq 0.39,\ K\ell_2 \simeq 0.11,\ p_1 = 3.7 \text{ bars}.$$

The σ values used in the calculations of ℓ_1 were $\sigma_1 = 0.389$nm, $\sigma_2 = 0.468$nm. Comparing the conditions for CH_4+ SF_6 with those for H_2+ Ar, it should be noted that they were quite similar. Because of the large increase in polarizability, as expected, the

Brillouin peaks of the recorded spectra were well-defined. Nevertheless, no significant fast mode contribution was detectable in either case. As shown in Fig. 4.4 and Fig. 4.5, for the spectra corresponding to the CH_4 base pressure of 6.3 bars, the identified frequency shifts of the spectral peaks agreed with the calculated results based on hydrodynamic theory. For spectra with the CH_4 base pressure of 3.7 bars, the observed frequency shifts did not differ significantly from the hydrodynamic prediction. Using the hard-sphere model, Campa again confirmed that, under the experimental conditions chosen above, no fast mode should be observed in these cases[31]. Furthermore, it was concluded that the conditions required for detection of the fast mode contribution for SF_6+CH_4 mixtures were unlikely to be achievable in practice.

A possible point of importance here is that the structures of the SF_6 and CH_4 molecules are more complicated than those of Ar and H_2, and the validity of the hard-sphere model may be questionable. However, because $m_{SF_6}/m_{Ar} \simeq 3.7$ and $m_{CH_4}/m_{H_2} \simeq 7.9$, the average velocity of both the SF_6 and CH_4 molecules are considerably lower ($\bar{v}_{Ar}/\bar{v}_{SF_6} \simeq 2$, $\bar{v}_{H_2}/\bar{v}_{CH_4} \simeq 2.8$). At the same time, the ℓ_1 values for SF_6+CH_4, which depend on the densities and the diameters of the particles, remain almost unchanged. It was consequently expected that deviations from the hard-sphere model should not be significant (i.e. because of the low density and slower speed of the particles in the medium, the collision time is much lower than the mean free time). The observed results also

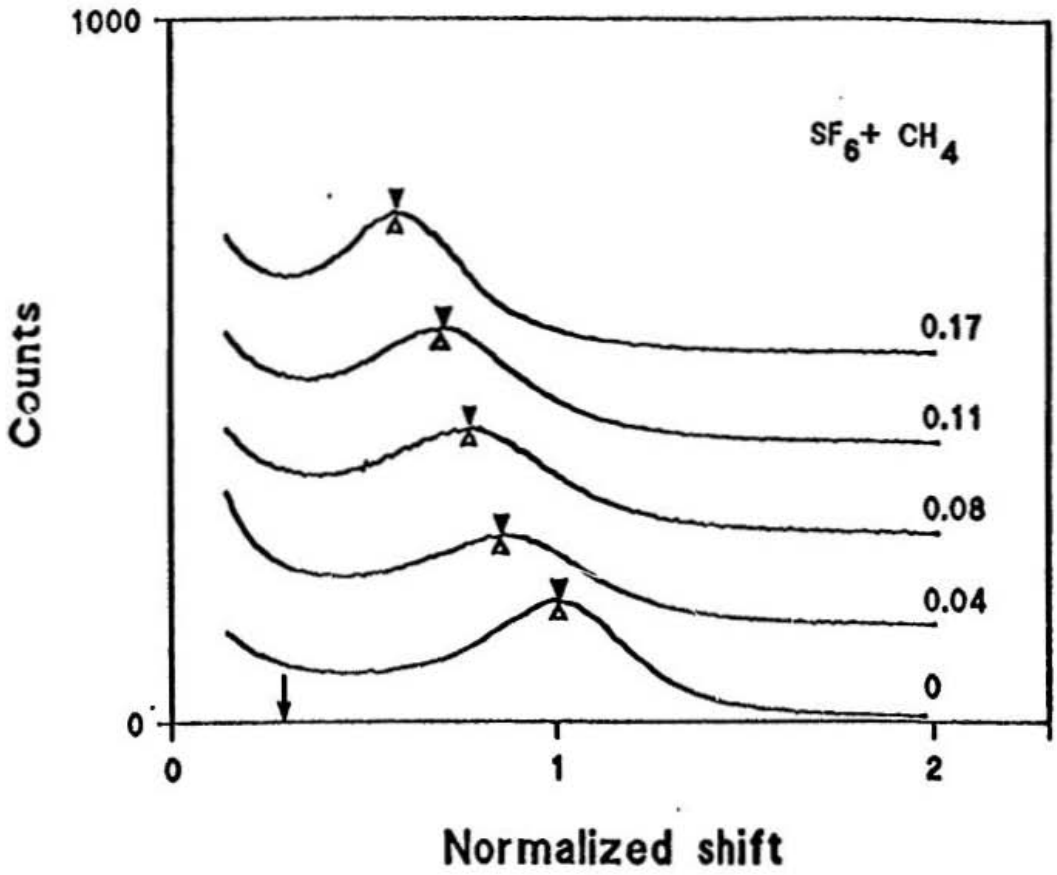

Fig. 4.4 Stokes spectra for SF_6+CH_4 mixtures with a fixed CH_4 partial pressure of 6.3 bars and fractional concentrations of SF_6 as listed. Each horizontal division represents frequency shift of 3.1GHz. The trianglar markers have the same meaning as in Fig. 4.1.

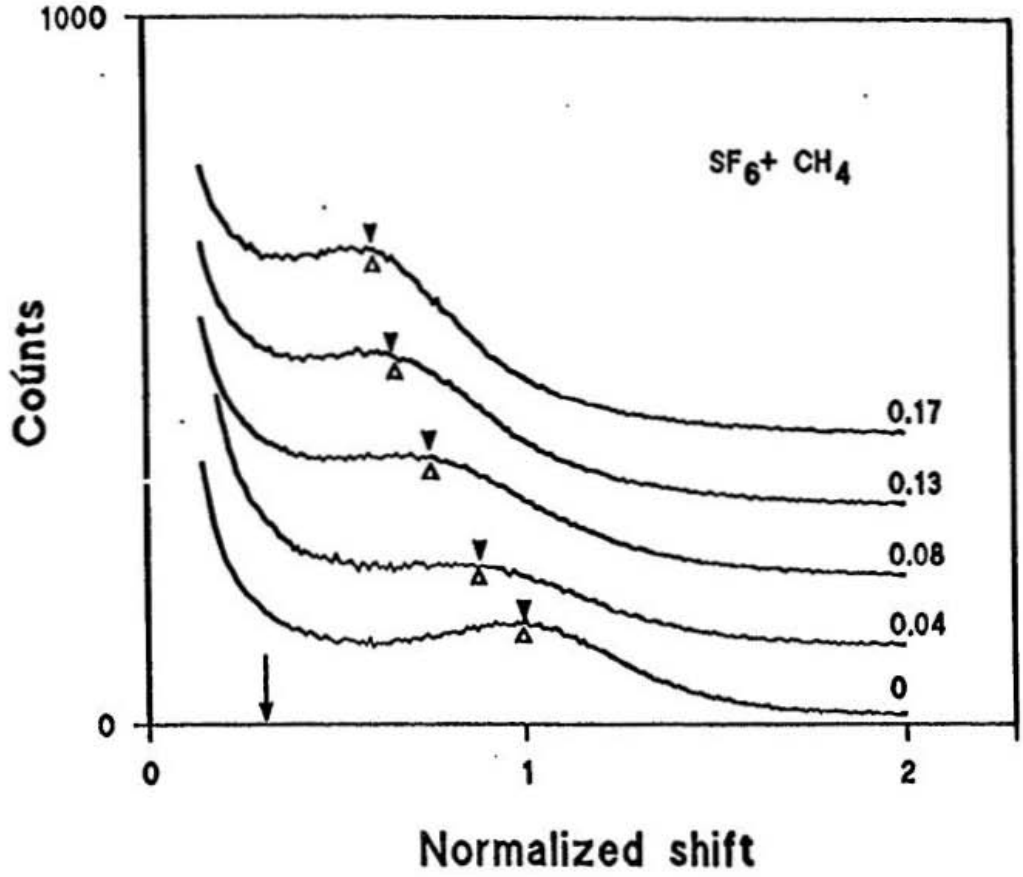

Fig. 4.5 Stokes spectra for SF_6+CH_4 with a fixed CH_4 partial pressure of 3.7 bars. See Fig. 4.4 for additional legend.

proved this. Hence the negative result for the SF_6+CH_4 mixture might be caused by a smaller m_2/m_1 ratio.

In the above two cases(H_2+Ar & SF_6+CH_4) the method used to characterize the experimental conditions for the gas mixtures with disparate masses (i.e. in terms of the ℓ_i values obtained using the conventional way) provides no insight into the distinctly different results. It was consequently decided to investigate alternate characterization criteria. The following discussion introduces an effective mean free path which provides a more consistent description.

§. 4.4 THE EFFECTIVE MEAN FREE PATHS DISCUSSION

First it is necessary to introduce the mean persistence ratio Ω_{ij}, which is defined as the mean ratio of the velocity component of particle i along its incident direction to its original velocity after a collision with a particle j. Ω_{ij} is given by [3]

$$\Omega_{ij} = \frac{1}{2}\left[M_i + M_i^2 M_j^{-1/2} \ln[(M_j^{1/2} + 1)/M_i^{1/2}] \right] \qquad (4.4)$$

where $M_i = m_i/(m_i + m_j)$, $(i,j = 1,2)$. m_i, m_j are the masses of two different particles, e.g. the H_2 molecules and Ar atoms in a binary gaseous system. Using (4.4), Ω_{ij} values were calculated for the studied mixtures. The results are listed in Table 4.3 where it

should be noted that, due to the large mass differences, $\Omega_{21} \simeq 1$ and $\Omega_{12} \simeq 0$, i.e. the velocity vector of a heavier particle almost does not change after it collides with a lighter particle, and the velocity vector of a lighter particle is totally changed after it collides with a heavier particle.

Table 4.3 The Mean Persistence Ratio for the Studied Mixtures

Ω_{ij}	H_2	Ar	CH_4	SF_6
H_2	0.406	2.64×10^{-2}	----	7.01×10^{-3}
Ar	0.937	0.406	----	----
CH_4	----	----	0.406	5.89×10^{-2}
SF_6	0.982	----	0.871	0.406

Given a particle of species i moving in the gas of species j, after a number of collisions with particles of species j, the velocity vector of particle i is randomized. The average number of collisions required for randomization, i.e. $\bar{n}_{ij}$, can be obtained using the Poisson distribution:

$$\bar{n}_{ij} = \frac{\sum_n n\Omega_{ij}^n}{\sum_n \Omega_{ij}^n} \qquad (i,j = 1,2) \qquad (4.5)$$

The calculated $\bar{n}_{ij}$ for the studied mixtures are given in Table 4.4.

As shown in Table 4.4, if the collisions occur between

identical particles, the velocity vector is randomized after less than two collisions ($\bar{n}_{11}$ = 1.68). If the collisions occur between unlike particles with large mass difference, the velocity of the lighter particles is greatly changed immediately after a collision with a heavier one, while the velocity vector of a heavier particle can be randomized only after a long series of collisions

Table 4.4 The Average Randomization Collision for the Studied Mixtures

$\bar{n}_{ij}$	H_2	Ar	CH_4	SF_6
H_2	1.68	1.03	----	1.01
Ar	15.9	1.68	----	----
CH_4	----	----	1.68	1.06
SF_6	54.6	----	7.73	1.68

with lighter particles. It should also be noted that unlike $\bar{n}_{12}$, $\bar{n}_{21}$ is very sensitive to the change of mass ratio m_2/m_1. Compared to the Ar+H_2 mixture, the mass ratio of the SF_6+CH_4 mixture decreases by roughly a factor of 2; $\bar{n}_{21}$ also decreases by a factor of 2 ($\bar{n}_{ArH_2}/\bar{n}_{SF_6CH_4} \simeq 2.1$).

For the picture to be complete, it must be recognized that in a binary mixture the collisions can occur not only between the different species but also between the same species. So instead of using Ω_{ij} in formula (4.8) it is more appropriate to use a

weighted mean persistence ratio as

$$\Omega_i = \frac{\ell_i}{\ell_{ii}} \Omega_{ii} + \frac{\ell_i}{\ell_{ij}} \Omega_{ij}, \qquad (4.6)$$

where ℓ_i, ℓ_{ij} are given by (1.4) and (1.5), respectively. This weighting scheme is chosen because, according to the definition of ℓ_i and ℓ_{ij}, the quantities ℓ_i/ℓ_{ii} and ℓ_i/ℓ_{ij} are the probabilities that a particle of species i collides with the particles of species i and j respectively. The average number of randomization collision $\bar{n}_i$ (i = 1,2) can therefore be calculated in a consistent way by substituting Ω_i for Ω_{ij} in the expression (4.5).

After an average of $\bar{n}_i$ collisions with both like and unlike particles, or in other words after moving an average distance of $\bar{n}_i \ell_i$, the velocity vector of a particle of species i is randomized. We can consequently define an <u>effective mean free path</u> given by

$$\bar{\ell}_{eff,i} = \bar{n}_i \ell_i / \bar{n}, \quad (i = 1,2) \qquad (4.7)$$

where the factor $\bar{n} = \bar{n}_{ii} = 1.68$, is used for normalization purposes to maintain consistency with the definition of the mean free path of a simple fluid. The effective mean free path $\ell_{eff,i}$ can be understood as the average distance that a particle of species i needs to travel before its velocity vector is

randomized. Consequently, if the wavelength of the density fluctuations to be probed is much larger than the effective mean free path for either species, the particles of both species should participate the propagation process, and hydrodynamic theory is expected to be valid. However, if one of the effective mean free paths is comparable to the wavelength of the perturbation to be probed, then deviations from hydrodynamic theory are expected. $K\bar{\ell}_{eff,i}$ (i=1,2) should provide the appropriate characterization of the conditions for a binary mixture, just like $K\ell_i$ is appropriate for a one-component fluid.

In order to test this point, the values of ℓ_i, $\ell_{eff,i}$ and $K\ell_{eff,i}$ (i=1,2) were calculated for Ar + H_2 mixtures with base H_2

Table 4.5 The Mean Free Paths and the Effective Mean Free Paths for Ar+H_2 Mixtures with a H_2 Base Pressure of 9.0 bars

x_2	ℓ_1(nm)	ℓ_2(nm)	$\ell_{eff,1}$(nm)	$\ell_{eff,2}$(nm)	$K\ell_{eff,1}$	$K\ell_{eff,2}$
0	11.3	----	11.3	----	0.271	----
0.04	11.0	3.00	10.8	25.7	0.259	0.616
0.10	10.4	2.92	9.85	22.7	0.236	0.544
0.13	10.1	2.89	9.44	19.3	0.226	0.462
0.16	9.80	2.85	9.05	17.8	0.217	0.427
0.18	9.55	2.82	8.70	16.5	0.208	0.395
0.21	9.31	2.78	8.38	15.5	0.201	0.371
0.23	9.08	2.75	8.07	14.5	0.193	0.347

Table 4.6 The Mean Free Paths and the Effective Mean Free Paths for Ar+H_2 Mixtures with a H_2 Base Pressure of 6.3 bars

x_2	ℓ_1(nm)	ℓ_2(nm)	$\ell_{eff,1}$(nm)	$\ell_{eff,2}$(nm)	$K\ell_{eff,1}$	$K\ell_{eff,2}$
0	16.1	----	16.1	----	0.386	----
0.05	15.4	4.24	15.1	34.8	0.362	0.834
0.10	14.8	4.16	14.1	30.2	0.338	0.724
0.14	14.2	4.09	13.3	26.8	0.319	0.642
0.17	13.7	4.02	12.5	24.1	0.300	0.578

pressures of 9.0 bars and 6.3 bars. These values are listed in Tables 4.5 and 4.6, respectively. It can be seen that the $\ell_{eff,1}$ values are almost equal to ℓ_1, but the $\ell_{eff,2}$ values are much larger than ℓ_2 in both cases. This can be understood in the following way. In these binary gas mixtures, due to the low concentration of Ar, the collisions experienced by a H_2 molecule are mostly between H_2 molecules themselves, even after some Ar atoms were added. On the contrary, the collisions experienced by an Ar atom are primarily with H_2 molecules. Because of the large mass ratio m_2/m_1, the motion of the Ar atom is hardly changed at all after such collisions. It is only after collisions with other Ar atoms or a series of collisions with H_2 molecules that the velocity vector of an Ar atom can be severely disturbed. So the effective mean free path for Ar is much larger than ℓ_2, which is the average distance between two successive collisions experienced

by an Ar atom. We also find that $\ell_{eff,2}$, the effective mean free path of Ar, is much larger than $\ell_{eff,2}$ for H_2. Comparing the $K\ell_{eff,i}$ values of Ar and H_2 (especially for lower Ar concentrations), $K\ell_{eff,2}$ is seen to be comparable to 1 while the $K\ell_{eff,1}$ values for H_2 are much smaller than 1. Thus as expected the dynamics of two components are partially decoupled. The sound mode probed in the experiment should therefore only be supported by the lighter species with a speed close to that for the single-component fluid (at the same temperature) obtained by removal of all the heavier species. Meanwhile the particles of the heavier species act like fixed scattering centers in the medium and severely damp the propagating fast sound mode. The observed spectral feature becomes broader and even unrecognizable as the concentration of Ar increases. It is concluded that characterization in terms of $K\ell_{eff,i}$ is consistent with the experimental results for this mixture, while characterization in terms of $K\ell_i$ is not.

Using the similar method, we obtained ℓ_i, $\ell_{eff,i}$ and $K\ell_{eff,i}$ (i=1,2) for SF_6+CH_4 mixtures. The data listed in Tables 4.7 and 4.8 correspond to SF_6+CH_4 mixture with CH_4 base pressure of 6.3 bars and 3.7 bars respectively. As we can see from Table 4.7 and 4.8, that there are some similarities between SF_6+CH_4 and Ar+H_2 mixtures. For instance, $\ell_1 \approx \ell_{eff,1}$ and $\ell_{eff,2}$ are much larger than ℓ_2 due to the low concentration of heavier particle and large mass ratio. However, in these cases the mass ratio m_2/m_1 is

Table 4.7 The Mean Free Paths and the Effective Mean Free Paths for SF_6+CH_4 Mixtures with a CH_4 Base Pressure of 6.3 bars

x_2	ℓ_1 (nm)	ℓ_2 (nm)	$\ell_{eff,1}$ (nm)	$\ell_{eff,2}$ (nm)	$K\ell_{eff,1}$	$K\ell_{eff,2}$
0	9.43	----	9.43	----	0.226	----
0.04	9.07	3.38	8.90	14.4	0.213	0.345
0.08	8.76	3.31	8.42	13.2	0.202	0.316
0.11	8.46	3.24	7.99	12.1	0.191	0.290
0.17	7.94	3.11	7.28	10.6	0.174	0.254
0.24	7.32	2.96	6.50	8.96	0.156	0.215
0.27	7.09	2.90	6.20	8.42	0.149	0.202

Table 4.8 The Mean Free Paths and the Effective Mean Free Paths for SF_6+CH_4 Mixtures with a CH_4 Base Pressure of 3.7 bars

x_2	ℓ_1 (nm)	ℓ_2 (nm)	$\ell_{eff,1}$ (nm)	$\ell_{eff,2}$ (nm)	$K\ell_{eff,1}$	$K\ell_{eff,2}$
0	16.2	----	16.2	----	0.388	----
0.08	15.0	5.66	14.4	22.1	0.345	0.530
0.12	14.3	5.51	13.4	20.0	0.321	0.479
0.17	13.7	5.37	12.6	18.1	0.302	0.434
0.20	13.2	5.23	11.9	16.3	0.285	0.391
0.23	12.6	5.10	11.3	15.1	0.271	0.362
0.30	11.6	4.80	9.91	13.1	0.237	0.314

roughly lowered by a factor of 2, so the average number of randomization collisions decreases considerably. as a result,

unlike the Ar+H_2 mixtures, $K\ell_{eff,1}$ and $K\ell_{eff,2}$ are no longer very different for SF_6+CH_4 mixtures. In the case with a CH_4 base pressure of 6.3 bars (Table 4.7), $K\ell_{eff,1}$ and $K\ell_{eff,2}$ are almost the same and small compared with 1. So the sound mode propagated in both components and no deviation from hydrodynamic theory was observed. In principle, a decrease in density might, as predicted by Campa[30], lead to the proper condition under which the sound mode is only supported by the lighter component (e.g. $K\ell_{eff,1} \ll 1$ and $K\ell_{eff,2} \approx 1$). Such an experiment would, however, be difficult to perform because of the low spectral intensity levels, and would probably not produce any more definitive results than for the case of the Ar+H_2 mixtures.

§. 4.5. THE SLOW SOUND MODE IN SF_6 + H_2 MIXTURES

As previously mentioned, for a fast sound mode to be present, it is necessary that the mass ratio m_2/m_1 be much larger than 1. Besides this, since the fast sound mode propagates exclusively in the lighter component, in order to observe the fast sound mode contribution, which is associated with the first term in relation (1.3), the polarizability of the lighter component should be large or at least comparable to that of the heavier component. In general, since $m_2 \gg m_1$ implies $\alpha_2 \gg \alpha_1$, the selection of such mixtures is very limited. On the contrary, however, it is quite easy to choose suitable mixtures in order to study the dynamical

behavior of the heavier component in disparate mass mixtures, because the large polarizabiliy of the heavier particle favors the observation of the third term in (1.3). On intuitive grounds the SF_6+H_2 mixture ($m_2/m_1 \simeq 73$) was consequently chosen for the investigation of a possible slow sound mode contribution. Because the intensity of scattered light contributed from each term in (1.3) is propotional to α_i^2 (or the cross product of α_1 and α_2), the large polarizability of SF_6 ($\alpha_{SF_6}/\alpha_{H_2} \simeq 5.8$) effectively reduces the contributions from the first and second terms in (1.3) to a negligible level. In other words, to a good approximation the scattered light is from the heavier species only. In this experiment the spectra were obtained by (the reverse of the previous procedure) introducing the heavy component into the cell first. The observed sound mode was identifiable without ambiguity as the only shifted feature in the spectrum and, as expected, it propagated exclusively in the heavier species with speeds much lower (almost constant) than those obtained using hydrodynamic theory (Fig 4.6). The conditions for the experiment were as follows:

$$0 \leq x_1 \leq 0.50,\ 0.11 \leq K\ell_2 \leq 0.59,\ 0.66 \leq K\ell_1 \leq 1.2,\ p_2 = 1.7 \text{ bar}.$$

Although some broadening caused by the damping effect of H_2 molecules is evident, compared with the $Ar+H_2$ mixtures, the damping is much weaker in this case.

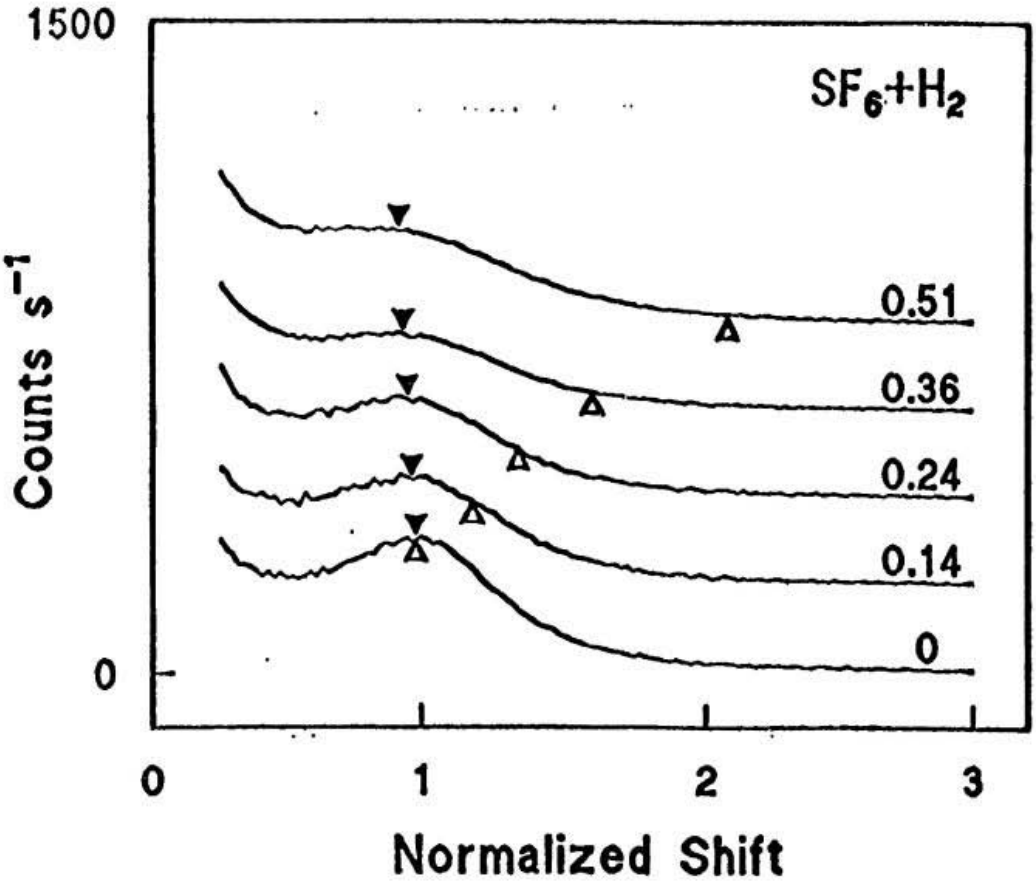

Fig. 4.6 Stokes spectra for SF_6+H_2 mixtures with a fixed SF_6 partial pressure of 1.7 bars and fractional concentrations of H_2 as listed. Each horizontal division represents frequency shift of 2.1Ghz. See Fig. 4.1 for additional legend.

In order to investigate the dynamic behavior of the SF_6+H_2 mixtures, the effective mean free paths were calculated as before. The calculated results corresponding to the above conditions are listed in Table 4.9. As the concentration of H_2 is increased ℓ_2 (the average distance between two successive collisions experienced by SF_6 molecules) decreases rapidly. However, this effect is due to increasing numbers of collisions between SF_6 and H_2, which hardly changes the velocity vector of the SF_6 molecules at all ($\bar{n}_{SF_6H_2} \simeq 54.6$), and $\ell_{eff,2}$ remains unchanged. It should also be noticed that $\ell_{eff,1}$ (the effective mean free path of H_2) is smaller than ℓ_1 (the average distance between two succesive collisions experienced by H_2 molecules). This can be explained in following way: when a H_2 molecule collides with a SF_6 molecule the collision is so "effective" that immediately after collision the velocity vector of the H_2 molecule changes greatly ($\bar{n}_{H_2SF_6} \simeq 1.01$). Therefore, although ℓ_1 is quite large for the mixtures with a very small amount of H_2 added, this effect brings the effective mean free path of H_2 down to almost the same value as that of SF_6. We can picture the situation as one where the sound wave is propagating in the heavier species SF_6 while the H_2 molecules are rapidly ($\bar{v}_{H_2} / \bar{v}_{SF_6} \simeq 8.5$) bounced back and forth between the SF_6 molecules. The situation here is quite different from that for the fast sound mode in Ar+H_2 mixtures. Although the dynamics of two components are no longer separated in the same sense, the sound mode is only supported b the heavy species, while the light particles act as small perturbations following the collective

Table 4.9 The Mean Free Paths and the Effective Mean Free Paths for SF_6+H_2 Mixtures with a SF_6 Base Pressure of 1.7 bars

x_1	ℓ_1 (nm)	ℓ_2 (nm)	$\ell_{eff,1}$ (nm)	$\ell_{eff,2}$ (nm)	$K\ell_{eff,1}$	$K\ell_{eff,2}$
0	----	24.6	----	24.6	----	0.589
0.07	48.4	18.6	29.8	24.4	0.714	0.585
0.14	45.5	14.9	28.6	24.1	0.685	0.578
0.19	43.0	12.5	27.6	23.9	0.661	0.573
0.24	40.7	10.7	26.7	23.6	0.640	0.566
0.27	38.6	9.37	25.6	23.5	0.613	0.563
0.35	35.1	7.53	24.2	23.1	0.580	0.554
0.42	32.1	6.27	22.7	22.6	0.544	0.542
0.47	29.6	5.37	21.4	22.2	0.513	0.532
0.50	27.5	4.72	20.3	21.8	0.486	0.522

motions of the heavy particles. Consequently little change in sound velocity is expected, as observed in Fig. 4.6. In reality the slow sound is not uncommon. One example is the sound mode in a piece of metal at room temperature where the sound is supported by the ions vibrating around the lattice points while the valence electrons act as a small perturbation which has little effect on the sound velocity.

§. 4.6. CONCLUSIONS

Under the experimental conditions predicted by the theory, a fast sound mode contribution to the light scattering spectrum of $Ar+H_2$ mixtures has been detected. Unlike the ordinary sound mode, the fast sound mode propagates only in the light component in the presence of the (essentially fixed) heavy scattering centers. It is the first time that a non-hydrodynamic mode in a fluid has been detected using the light scattering technique.

An analogous slow sound mode contribution to the spectra of SF_6+H_2 mixtures has been clearly identified. It is concluded that this mode is, in general, much more readily observable due to the highly favorable polarizability ratio and considerably weaker acoustic attenuation caused by the light component.

A new parameter called the effective mean free path was introduced in order to obtain a more consistent characterization of the dynamical behavior in binary mixtures with disparate masses. In particular, this has made it possible to more clearly understand why the fast sound mode was not detected in mixtures of SF_6+CH_4 under conditions similar to those for $Ar+H_2$ (where the fast mode was detected). It is most probable that the effect is due to the decreased mass ratio (m_2/m_1) for the case of the SF_6+CH_4 mixtures.

REFERENCES:

[1]. A. Anderson, *The Raman Effect 1* (Marcel Dekker Inc., New York, 1971)

[2]. L. Landau and S. Lifshitz, *Electrodynamics of Continuous Media*, (Addision Wesley Publishing Company, Inc., Reading, Massachusetts, 1960)

[3]. S. Chapman, and T. G. Cowling, *The Mathematical Theory of Non-uniform Gases*, (Cambridge University Press, London, 1970)

[4]. J. P. Boon and S. Yip, *Molecular Hydrodynamics*, (McGraw-Hill International Book Company, 1980)

[5]. H. Grad, *Rarefied Gas Dynamics*, edited by F. M. Deviene (Pergamon, New York, 1960), Vol. 3, p.100

[6]. R.J. Huck, and E. A. Johnson, *Phys. Rev. Lett.*, 44,142(1980)

[7]. J. R. Bowler, and E. A. Johnson, *Phys. Rev. Lett.* 54,329 (1985)

[8]. Bosse, G. Jacucci, and M. Ronchetti, *Phys. Rev. Lett.*,

57,3277 (1986)

[9]. W. Montfrooij, P. Westerhuijs, V. O. de Haan, and I. M. de Schepper, *Phys. Rev. Lett.*, 63,544(1989)

[10]. A. Campa and E. G. D. Cohen, *Phys. Rev., A* 39,4909(1989)

[11]. W. S. Gornall, C. S. Wang, C. C. Yang, and N. Bloembergen, *Phys. Rev. Lett.*, 26,1094(1971)

[12]. N. A. Clark, *Phys. Rev. A*, 12,232(1975)

[13]. N. A. Clark, *Phys. Rev. A*, 12,2092(1975)

[14]. L. Letamendia, J. P. Chabrat, G. Nouchi, J. Rouch, C. Vaucamps and S. H. Chen, *Phys. Rev. A*, 24,1574(1980)

[15]. R. Zwanzig, *Annual Rev. of Phys. Chem.*, 16,67(1965)

[16]. I. L. Fabelinskii, ***Molecular Scattering of Light***, (Plenum Press, New York, 1968)

[17]. R. Pecora, *J. Chem. Phys.*, 40,1604(1964)

[18]. B. Chu, ***Laser Light Scattering***, (Academic Press, 1974)

[19]. L. E. Reichl, ***A Modern Course in Statistical Physics***, (University of Texas Press, Austin, 1986)

[20]. R. D. Mountain and J.M. Deutch, ***J. Chem. Phys.***, 50,1103 (1969)

[21]. L. Landau and E. Lifshitz, ***Fluid Mechanics***, (Addison-Wesley Publications. Co., Inc., Reading, Mass., 1959)

[22]. A. Campa, Ph. D. thesis, The Rockefeller Univ. 1989

[23]. A. Campa, and E. G. D. Cohen, ***Phys. Rev. A***, 41,5451(1989)

[24]. S. F. Ahmad , Ph. D. thesis, Memorial University of Newfoundland.

[25]. W. May, H. Kiefte, M. J. Clouter, and G. I. A. Stegeman, ***Appl. Opt.***, 17,1603(1978)

[26]. M. J. Clouter, H. Kiefte, and C. G. Deacon, ***Phy. Rev. A***, 33,2749(1986)

[27]. J. A. Zollweg, (private communication 1990), School of Chemical Engineering, Cornell University.

[28]. D. Tabor, ***Gases, Liquids and Solids***, (Penguin Book Inc.,

Baltimore, Maryland)

[29]. J. G. Hayden and J. P. O'Connell, *Ind. Eng. Chem. Process. Des. Dev.* 14,209(1975)

[30]. M. J. Clouter, H. Luo, H. Kiefte and J. A. Zollweg, *Phys. Rev. A*, 41,2239(1989)

[31]. A. Campa (private communications, 1990), The Rockefeller University.

Light scattering in gas mixtures: Evidence of fast and slow sound modes

M. J. Clouter, H. Luo, and H. Kiefte
Department of Physics, Memorial University, St. John's, Newfoundland, Canada A1B 3X7

J. A. Zollweg
School of Chemical Engineering, Cornell University, Ithaca, New York 14853
(Received 30 October 1989)

Campa and Cohen [Phys. Rev. A 39, 4909 (1989)] have predicted that dilute, binary mixtures of gases with disparate masses should exhibit a (fast) sound mode whose velocity is considerably greater than expected on the basis of conventional hydrodynamic theory, and which should be observable via light-scattering experiments. Effects that are consistent with this prediction were observed in the Brillouin spectra of the H_2+Ar system, but were not detected for the case of CH_4+SF_6. Results for the SF_6+H_2 mixture demonstrate the existence of an analogous slow-mode contribution to the spectrum.

The suggestion[1] that a fast sound mode can exist in binary mixtures of noble-gas *liquids* when the two molecular species have widely different (i.e., disparate) masses has been confirmed by neutron-scattering experiments,[2] which are capable of probing the appropriate wave-vector regime. More recently[3] it has been proposed that the corresponding effect should also be present in binary mixtures of *gases* at low density and in the wave-vector regime accessible by light-scattering techniques. The Brillouin scattering experiments and calculations described in this paper provide evidence for the existence of a fast-mode contribution in the spectrum of H_2+Ar mixtures which, however, is difficult to detect. Spectra of CH_4+SF_6 as obtained under comparable conditions did not exhibit a similar behavior. By comparison, corresponding effects which can be identified with an analogous slow-mode contribution to the spectrum were found to be readily observable in the case of SF_6+H_2 mixtures.

The fast mode is interpreted[4] as one which propagates only in the lighter of the two species when the mole fraction of the heavier species is relatively low (≤ 0.3) and under conditions which conform to the approximate criterion $kl_1 \sim kl_2 \sim 1$, where l_1 is the mean free path for the lighter species, l_2 is the mean free path for the heavier species, and $k = 2\pi/\Lambda$ is the wave number of the sound being probed. One thus envisions an experiment where the sample cell is first charged with a fixed number density of the lighter species which is high enough so that a well-defined Brillouin peak is observed in the scattered-light spectrum, and this spectrum is subsequently monitored as successive increments of the heavier species are added. Qualitatively, the predicted[3,4] behavior (for low concentrations of the heavier species) is that a spectral peak will persist at a position (frequency shift) which is *not* determined by the density of the mixture as normally expected, but which remains substantially unchanged. This is indicative of a *fast* sound mode which continues to propagate in the lighter species only. One expects, however, that the heavier species will contribute to the attenuation of this mode, so that the observed spectral feature will become broader and perhaps unrecognizable.

Given that the minimum value of the probed wavelength Λ in a Brillouin scattering experiment is $\sim$250 nm (at a scattering angle of 180°), it turns out that the appropriate conditions can be satisfied for mixture pressures of order 10 bar or less, provided the mole fraction x_2 of the heavier species is kept sufficiently small. There is, however, the observational requirement that the permissible range of x_2 values be large enough so that the corresponding changes in the mean density of the mixture give rise to readily measurable changes in the characteristics of sound propagation that are normally expected for a mixture, e.g., the velocity. Otherwise, a possible fast-mode contribution to the spectrum would not be distinguishable from the (normal) contribution of the mixture. With the above constraint on Λ, this dictates that in most cases the partial pressure of the lighter species should be kept as low as possible while maintaining a readily detectable Brillouin signal.

In the theoretical formulation of the problem[3,4] the scattered light intensity is expressed as a sum of three contributions, the first two of which are associated respectively with the lighter and heavier species alone, while the third is a mixed term

$$I(k,\omega) \sim a_1^2 x_1 S_{11}(k,\omega) + a_2^2 x_2 S_{22}(k,\omega) + 2a_1 a_2 \sqrt{x_1 x_2} S_{12}(k,\omega). \quad (1)$$

Here the S_{ij} are partial dynamic structure factors, a_i are molecular polarizabilities, the x_i are mole fractions, and k (as above) and ω are the probed wave number and angular frequency, respectively. Throughout the remainder of this paper we adhere to the convention established for this equation, whereby the subscripts 1 and 2 refer to the lighter and heavier species, respectively. It is clear from Eq. (1) that, for given x_i, the a_i values are important in determining which (if any) of the three contributions will dominate the spectrum. In particular (while recognizing

that heavier molecules have generally higher polarizabilities), observation of the fast-mode associated with the first term is facilitated by an a_1 value that is at least comparable to a_2. The combination of H_2 and Ar, with a mass ratio of 1:20, represents a reasonable compromise in this respect ($a_2/a_1 \simeq 2$),[5] and it is this suggested[3] mixture that was chosen for initial investigations. As mentioned above, experiments were also performed with the mixtures CH_4+SF_6 and SF_6+H_2. In the latter case emphasis was placed on investigation of the slow-mode contribution corresponding to the second term in Eq. (1).

The spectra were obtained using incident radiation provided by an Ar^+ laser (Coherent Radiation Innova Model 90-5) operating in a single-cavity mode with a nominal wavelength (λ_0) of 514.5 nm and a power output in the range 300-500 mW. The spectrometer consisted of a scanning Fabry-Pérot interferometer (Burleigh Model RC-110), a cooled photomultiplier detector (ITT FW130), photon counting electronics, and a combined data-acquisition and Fabry-Pérot control system (Burleigh Model DAS-1). The scattered radiation was prefiltered (using a grating monochromator) to reject unwanted Raman radiation, and the spectra were obtained by a repetitive scanning process with accumulation times ranging from 5 to 24 h. All experiments were performed at room temperature (293 K) using a sample cell which permitted a choice between scattering angles (θ) of 157.5° and 22.5°. The former angle was used in most experiments and corresponds to a probed wavelength $\Lambda = 2\lambda_0/\sin(\theta/2) = 262$ nm. Pressures were measured via Bourdon-tube gauges with an estimated accuracy of ± 0.05 bar, and particular care was taken to ensure that all gases were properly mixed before the spectral accumulation process was begun.

As implied above, the criterion used to detect a fast-mode contribution to a given spectrum was to compare the frequency shift of the observed spectral peak with that determined from the well-known Brillouin equation, $\omega_B = 4\pi(v_s/\lambda_0)\sin(\theta/2)$, where the sound speed v_s for the mixture is calculated in the limit $k \to 0$ via the basic relation $v_s = (V_m/M\kappa_s)^{1/2}$. Here V_m is the molar volume of the mixture, M is the average molecular weight, and κ_s is the adiabatic compressibility. For mixtures of components with very different molecular weights, the largest correction to the ideal-gas value for the sound speed is due to the molecular weight of the mixture being different from that calculated on the basis of partial pressures. Consequently, the measured pressures were first used to calculate different mixture compositions (i.e., the x_i's) via the virial equation of state, with terms involving virial coefficients beyond the second being ignored. Second virial coefficients were calculated using the method of Hayden and O'Connell.[6] For each series of experiments (where different mixture compositions were obtained by incremental addition of one species to an initially pure sample of the other species), the molar volume of the initially pure component at the initial pressure was calculated first. The x_i's for subsequent mixture compositions were then determined subject to the constraint that the partial volume of the initial pure component maintain its original value. Sound speeds were calculated using the virial form,

$$v_s^2 = \frac{RT}{M}\left(1+\frac{Bp}{RT}\right)^2\left[1-R\left(1+\frac{p}{R}\frac{dB}{dT}\right)^2 \times\left(C_p^0-pT\frac{d^2B}{dT^2}\right)^{-1}\right]^{-1}, \quad (2)$$

where p is the (total) pressure, C_p^0 is the ideal-gas heat capacity, and B is the second virial coefficient for the mixture.

The values of kl_1 and kl_2, which are used to characterize the sample conditions, were calculated using the following expression[4] for the mean free paths in a binary mixture:

$$l_i^{-1} = \sqrt{2}\pi n_i\sigma_i^2 + (1+m_i/m_j)^{1/2}\pi n_j\sigma_{ij}^2. \quad (3)$$

Here n_i and n_j are the partial number densities, σ_i and σ_j are the hard-sphere diameters for the two species of mass m_i and m_j, and $\sigma_{ij} = (\sigma_i+\sigma_j)/2$.

H_2+Ar

Spectra for this mixture were obtained for three different base pressures p_1 of H_2. The σ values (in nm) that were used in the calculations were $\sigma_1 = 0.297$,

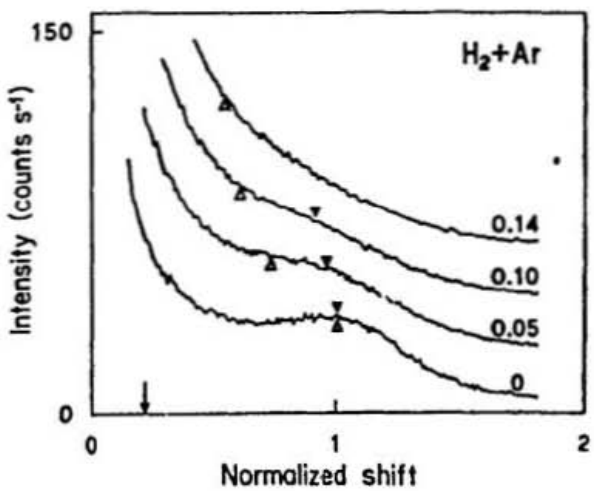

FIG. 1. Selected scattered-light spectra for mixtures of H_2 and Ar with a fixed H_2 partial pressure (p_1) of 6.3 bars, and fractional concentrations (x_2) of Ar as indicated. The central Rayleigh peak has been removed to permit stacking of the spectra on an appropriate scale. Only the (Stokes) region of downshifted frequencies is shown, with the frequency shifts normalized to unity at the position of the Brillouin peak for $x_2 = 0$. The solid triangles indicate the estimated peak positions of the observed Brillouin features, while the open triangles designate the normalized shifts that were calculated (see text) for $k \to 0$. The arrow indicates the position of the Brillouin peak for $x_2 = 1$. The scattering angle was 157.5°.

$\sigma_2 = 0.340$. The mixture conditions are listed as follows:

$0 \leq x_2 \leq 0.25$, $0.27 \geq kl_1 \geq 0.21$, $kl_2 \simeq 0.07$, $p_1 = 9.0$ bars,

$0 \leq x_2 \leq 0.18$, $0.32 \geq kl_1 \geq 0.27$, $kl_2 \simeq 0.09$, $p_1 = 7.7$ bars,

$0 \leq x_2 \leq 0.17$, $0.39 \geq kl_1 \geq 0.33$, $kl_2 \simeq 0.10$, $p_1 = 6.3$ bars.

Evidence of a fast-mode contribution to the spectrum in the lower part of the x_2 range was observed in all three cases. The best results were obtained for $p_1 = 6.3$ bars, and this case is shown in Fig. 1. Here it can be seen that, while a distinct spectral feature is identifiable only for $x_2 \leq 0.1$, it is nevertheless apparent that the peak position on the scale of normalized frequency shifts remains essentially unchanged with increasing x_2, and differs considerably from the calculated $(k \to 0)$ values as described above. This behavior is consistent with theoretical predictions.[3,4] The obvious difficulty experienced in detecting the fast-mode contribution as a well-defined spectral feature is most probably associated (i) with a relative polarizability a_2/a_1 that favors the dominance of the second and third terms in Eq. (1) and (ii) with the low absolute value of a_1 leading to low signal levels in the density range of interest. Investigations of the CH_4+SF_6 mixture were undertaken with the latter point in mind.

CH_4+SF_6

The polarizability[5] of CH_4 is approximately three times greater than that of H_2 so that lower p_1 values are accessible while maintaining a strong signal. The value[7,8] of a_1/a_2 for this mixture is very nearly the same as for the H_2+Ar case, while $m_2/m_1 = 9$ is lower by roughly a factor of 2. The hard-sphere diameters used in the calculations were (in nm) $\sigma_1 = 0.389$, $\sigma_2 = 0.468$. Spectra were recorded for two values of p_1 (in bars) as follows:

$0 \leq x_2 \leq 0.27$, $0.23 \geq kl_1 \geq 0.17$, $kl_2 \simeq 0.07$, $p_1 = 6.3$ bars

$0 \leq x_2 \leq 0.30$, $0.39 \geq kl_1 \geq 0.28$, $kl_2 \simeq 0.11$, $p_1 = 3.7$ bars.

It should be noted that conditions for the lower p_1 case are similar to those of Fig. 1 for H_2+Ar. Nevertheless, no significant fast-mode contribution was detectable in either case; i.e., the observed frequency shifts of the spectral peak did not differ significantly from the values calculated for $k \to 0$. An understanding of this result must await future theoretical calculations: perhaps the mass ratio is too low for the effect to be observable.

SF_6+H_2

This mixture, with $m_2/m_1 = 73$, was chosen for the investigation of a possible slow-mode contribution associated with the second term in Eq. (1). On intuitive grounds, this contribution was presumed to be observable in the same regime of kl_1 and kl_2 values as above, but with $x_1 \leq 0.3$. The mixture takes advantage of a large disparity in polarizability $(a_2/a_1 \simeq 6)$ which favors the dominance of the S_{22} term of Eq. (1). In fact, for the noted range of x_1 values, this large polarizability effect can be expected to reduce the contributions from the first and third terms of Eq. (1) to a negligible level. In other words, to a good approximation the experiment is sensitive to light scattering from the heavier species only, and any mode which propagates exclusively in this species should be identifiable without ambiguity as the only (shifted) feature in the spectrum. The wide separation between the Brillouin shifts for $x_2 = 1$ and $x_2 = 0$ is also of importance in this connection. The conditions for two separate experiments were as follows:

$0 \leq x_1 \leq 0.50$, $0.59 \geq kl_2 \geq 0.11$, $1.2 \geq kl_1 \geq 0.66$, $p_2 = 1.7$ bars,

$0 \leq x_1 \leq 0.84$, $0.74 \geq kl_2 \geq 0.03$, $1.3 \geq kl_1 \geq 0.23$, $p_2 = 1.3$ bars.

The first case is shown in Fig. 2 where it is clear that, although some broadening is evident, a distinct spectral feature persists over the complete range of x_1 values investigated. In view of the above comments, there can consequently be no doubt that a well-defined mode exists which propagates exclusively in the heavier species. Furthermore, the frequency shift of the peak is essentially independent of x_1, and a large discrepancy develops between the observed and calculated $(k \to 0)$ values of the shift at the upper limit of x_1. Although the theory[3,4] has not yet been applied to elucidating the properties of this (slow) mode, it can be assumed by analogy with the fast-mode predictions that qualitative agreement exists. It remains to be seen whether agreement is preserved in matters of detail.

Figure 3 represents a further investigation of this phenomenon with the principal differences being (i) that the scattering angle was changed from 157.5° to 22.5°, thereby probing a range of k values which is lower by a factor of ~ 4, and (ii) that a wider range of x_1 values was employed. Although the wave-vector regime is less favorable, it is nevertheless clear that the effect persists for low values of x_1, with the observed peak position conforming to the calculated $(k \to 0)$ value only at the upper limit of

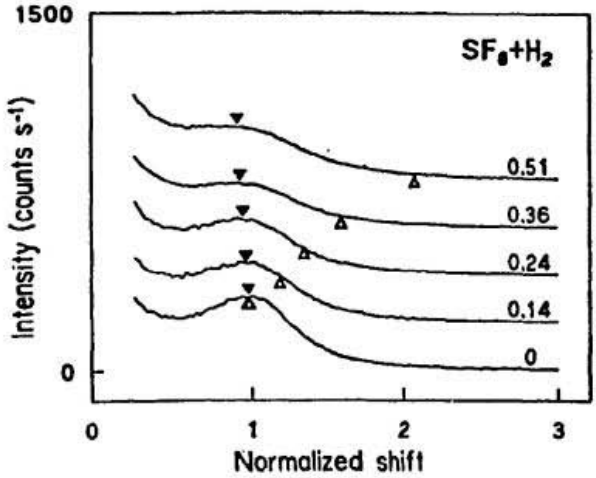

FIG. 2. Stokes spectra for SF_6+H_2 with a fixed SF_6 partial pressure (p_2) of 1.7 bars and fractional concentrations (x_1) of H_2 as listed. The scattering angle was 157.5°. The Brillouin peak for $x_1=1$ occurs at a normalized shift of 8.5. The triangular markers have the same meaning as in Fig. 1.

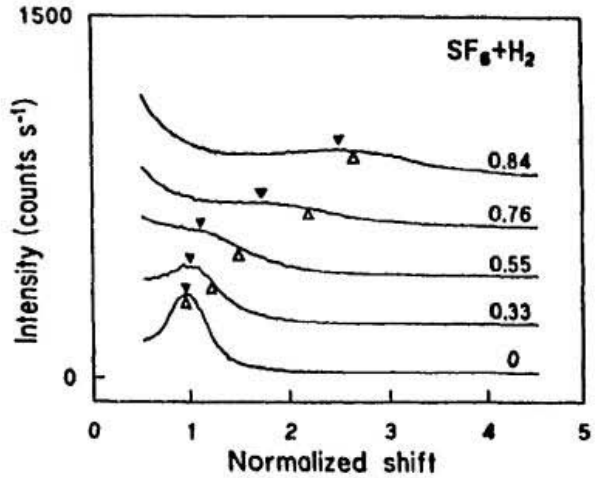

FIG. 3. Stokes spectra for the same mixture as in Fig. 2, but with $p_2=1.3$ bars and a scattering angle of 22.5°. The triangular markers have the same meaning as in Figs. 1 and 2.

x_1 where the third term in Eq. (1) begins to play a dominant role.

In brief, a fast-mode contribution to the light-scattering spectrum of H_2+Ar mixtures has been detected under conditions predicted by theory. The negative result obtained for CH_4+SF_6 mixtures raises the question of what is meant by *disparate* masses, i.e., what is the minimum value of m_2/m_1 required for the effect to be observable? One might also question whether the hard-sphere model of the theory is applicable for this mixture. An analogous slow-mode contribution to the spectrum of SF_6+H_2 mixtures has been clearly identified, and it is concluded that this mode is, in general, much more readily observed because of the highly favorable polarizability ratios that can be achieved for a variety of different mixtures.

The authors wish to thank Professor E. G. D. Cohen for suggesting this problem, for many illuminating discussions, and for a critical reading of the manuscript.

[1]A. Campa and E. G. D. Cohen, Phys. Rev. Lett. **61**, 853 (1988).
[2]W. Montfrooij, P. Westerhuijs, V. O. de Haan, and I. M. de Schepper, Phys. Rev. Lett. **63**, 544 (1989).
[3]A. Campa and E. G. D. Cohen, Phys. Rev. A **39**, 4909 (1989).
[4]A. Campa, Ph. D. thesis, The Rockefeller University, 1989.
[5]J. O. Hirschfelder, C. F. Curtis, and R. B. Bird, *Molecular Theory of Gases and Liquids* (Wiley, New York, 1964).
[6]J. G. Hayden and J. P. O'Connell, Ind. Eng. Chem. Process. Des. Dev. **14**, 209 (1975).
[7]$\alpha_2=50\times10^{-25}$ cm^3 (for SF_6) was determined via the Lorentz-Lorenz relation using density and refractive index data from Ref. 8.
[8]H. Kiefte, R. Penney, and M. J. Clouter, J. Chem. Phys. **88**, 5846 (1988).